

Journal of Mechanics of Materials and Structures

LINEAR BUCKLING ANALYSIS OF CRACKED PLATES BY SFEM AND XFEM

Pedro M. Baiz, Sundararajan Natarajan, Stéphane P. A. Bordas, Pierre Kerfriden
and Timon Rabczuk

Volume 6, No. 9-10

November–December 2011



mathematical sciences publishers

LINEAR BUCKLING ANALYSIS OF CRACKED PLATES BY SFEM AND XFEM

PEDRO M. BAIZ, SUNDARARAJAN NATARAJAN,
STÉPHANE P. A. BORDAS, PIERRE KERFRIDEN AND TIMON RABCZUK

In this paper, the linear buckling problem for isotropic plates is studied using a quadrilateral element with smoothed curvatures and the extended finite element method. First, the curvature at each point is obtained by a nonlocal approximation via a smoothing function. This element is later coupled with partition of unity enrichment to simplify the simulation of cracks. The proposed formulation suppresses locking and yields elements which behave very well, even in the thin plate limit. The buckling coefficient and mode shapes of square and rectangular plates are computed as functions of crack length, crack location, and plate thickness. The effects of different boundary conditions are also studied.

1. Introduction

Plate-like structures (thin-walled structures) are one of the most widely used structural elements in advanced engineering design, particularly in the aerospace industry. In order to efficiently study such structures, different plate theories have been proposed during the years. In classical plate theory (also known as Kirchhoff) the shear deformation through the plate thickness is neglected because of the assumption that the normal to the middle surface remains normal after deformation. Although for most practical applications this theory is sufficient, it has been proved (see references [5] and [6] in [Reissner 1947]) that the Kirchhoff theory of thin plates is not in accordance with experimental results for problems with stress concentration — stresses at an edge of a hole when the hole diameter is of the same order of magnitude as the plate thickness — or in the case of composite plates, where the ratio of the Young's modulus to the shear modulus can be very large (low transverse shear modulus compared to isotropic materials). In shear deformable plate theory (also referred to as Mindlin or Reissner), it is assumed that the normal-to-the-middle surface will not necessarily remain perpendicular after deformation, adding rotations of the normal as extra unknowns into the partial differential equations, and therefore overcoming problems associated with the application of the classical theory.

A plate structure may lose its ability to withstand external loading when the stored compressive membrane strain energy reaches a critical level. This phenomenon, known as buckling, is characterised by sudden and disproportionate large displacements that could lead to structural failure. In the presence of flaws such as through-the-thickness cracks, critical buckling loads will decrease as a result of the local flexibility provided by the crack, severely affecting the performance of the plate structure. Buckling analysis of isotropic cracked panels has been conducted by researchers analytically and numerically. In

The support of the Royal Academy of Engineering/Leverhulme Trust for Bordas' senior research fellowship is gratefully acknowledged.

Keywords: Mindlin, Reissner, shear deformable plate theory, buckling, partition of unity methods (PUM), extended finite element method (XFEM), fracture.

[Stahl and Keer 1972] homogeneous Fredholm integral equations of the second kind were used to solve the eigenvalue problem for cracked plates under compressive loading. Buckling of cracked elastic plates subjected to uniaxial tensile loads was presented in [Markström and Storåkers 1980]. More recently, in [Brighenti 2009] the effects of crack length and orientation on the buckling loads of rectangular elastic thin plates under different boundary conditions were shown, and similarly in [Alinia et al. 2007] for analysis of panels containing central or edge cracks under shear loading, both using the finite element method (FEM). Numerical approaches not based on FEM that address the eigenvalue problem of cracked plates under compressive loading include those of [Liu 2001] using the differential quadrature element method and [Purbolaksono and Aliabadi 2005] using the dual boundary element method. Other works dealing with buckling of cracked plates are [Sih and Lee 1986; Riks et al. 1992; Vafai et al. 2002].

Nowadays, it is well accepted that engineers need to resort to numerical approaches to solve a wider range of practical problems. FEM is the most widely used numerical technique in industry to solve structural problems and a wide range of commercially packages are currently available. Despite its robustness and versatility, FEM efficiency in modelling cracks, discontinuities, and areas of high stress concentration has always been considered an area for improvement since a very refined discretisation is typically necessary in order to obtain accurate solutions. If the discontinuity is moving or is located within a complex geometry, the task of obtaining an acceptable mesh could become very cumbersome and extremely time-consuming.

Extended FEM (XFEM) [Belytschko and Black 1999], which is based on a standard Galerkin procedure and employs the concept of partition of unity proposed in [Babuška et al. 1994], can accommodate the internal boundaries of a crack without regenerating the mesh around the discontinuity. The basic concept behind the method is the incorporation of special local enrichment functions into a standard FEM approximation. Recent areas of XFEM application cover a wide range of scientific and engineering problems, including fracture, dislocations, inclusions, grain boundaries, phase interfaces, multiscale, among others (see [Belytschko et al. 2009] for a recent review). In the particular case of plate bending, the first work on fracture of plates with XFEM was [Dolbow et al. 2000] while in [Areias and Belytschko 2005] a general nonlinear XFEM formulation for analysis of shells was presented. Wyart et al. [2007] presented a mixed-dimensional approach (shell/3D XFEM) for accurate analysis of cracks in thin-walled structures and Bordas et al. [2009] presented applications of strain smoothing in finite element problems with discontinuities and singularities for 2D, 3D, and plate/shell formulations (smoothed extended finite element method (SmXFEM)). In terms of eigenvalue problems, [Bachene et al. 2009; Natarajan et al. 2009b] presented an application of XFEM for the study of the linear vibration of cracked isotropic plates. Other recent works dealing with cracks in thin-walled structures are [Rabczuk and Areias 2006; Rabczuk et al. 2007; 2010].

The strain smoothing concept within FEM (SFEM) was recently proposed in [Liu et al. 2007a], and since then a series of publications addressing the properties and applications of the method in a variety of structural mechanics problems have been presented. Some of the recent papers on the area include: its mathematical foundations [Liu et al. 2007b; Nguyen-Xuan et al. 2008a; Bordas and Natarajan 2010], plate [Nguyen-Xuan et al. 2008b] and shell [Nguyen-Thanh et al. 2008] analyses, limit analysis [Le et al. 2010], and polygonal meshes [Dai et al. 2007]. The main idea behind SFEM is to split a finite element into subcells over which the gradients (strains) are smoothed. If a constant smoothing function is used over each subcell, the area integration can be recast into a line integration along its edges. This allows

for field gradients to be computed directly by only using the shape functions (no derivatives of shape functions are needed), which accordingly reduces the requirement on the smoothness of shape functions. Some of the major advantages of SFEM that have been shown in the literature include: insensitivity to mesh distortion, lower computational cost than FEM for the same accuracy level, flexibility (by offering elements ranging from the standard FEM to quasiequilibrium FEM), insensitivity to locking for low numbers of subcells, and the possibility of constructing arbitrary polygonal elements. This field of research has led to the development of related approaches such as node-based SFEM [Liu et al. 2009b] and edge-based smoothed FEM for 2D problems [Liu et al. 2009a] (called face-based smoothed FEM for 3D problems). Following all these new developments, very recently in [Liu 2010a; 2010b] a theoretical framework was presented to unify the formulation of element-based and mesh-free methods; it attempts to improve the accuracy and efficiency of numerical solutions by using incompatible formulations based on a weakened weak form.

All the above mentioned developments illustrate the great potential of XFEM, particularly when combined with strain smoothing techniques [Bordas et al. 2009]. Some of the areas of improvement that strain smoothing could provide for XFEM are simplifying integration of discontinuous functions by replacing domain integration by boundary integration (see also [Natarajan et al. 2009a; 2010] for techniques suppressing the need for subcells for the integration of discontinuous approximations) and increasing stress and stress intensity factor accuracy.

The present paper is inspired by recent developments that show how curvature smoothing coupled with partition of unity enrichment can produce a plate element capable of cracking which is significantly more accurate than formerly proposed elements [Bordas et al. 2009]. This work attempts specifically to investigate the possibilities of smoothed XFEM for linear plate buckling and the effect of using the smoothing operator for the higher-order terms in the plate buckling equation. First a recently developed curvature strain smoothing plate bending element [Nguyen-Xuan et al. 2008b] is used to study the linear plate buckling phenomena (eigenvalue problem). Then, XFEM is used to obtain critical buckling loads of cracked isotropic shear deformable plates. Finally, the SmXFEM [Bordas et al. 2009] approach is applied to the linear buckling problem of cracked Mindlin–Reissner plates. Some of these approaches have been previously introduced by the authors in the context of free vibration analysis of cracked plates [Natarajan et al. 2009b], but until now the application of SFEM, XFEM, and SmXFEM has not been attempted in the area of linear plate buckling.

2. Mindlin–Reissner plate buckling

2.1. Basic problem formulation. Let Ω be the domain of a flat isotropic homogeneous thick plate, Γ the boundary, and h the thickness. The midplane of the plate is taken as the reference plane, see Figure 1.

The basic assumption for displacements is

$$\begin{Bmatrix} u(x, y, z) \\ v(x, y, z) \\ w(x, y, z) \end{Bmatrix} = \begin{Bmatrix} z\beta_x(x, y) \\ z\beta_y(x, y) \\ w(x, y) \end{Bmatrix}, \tag{1}$$

where $u(x, y, z)$, $v(x, y, z)$, and $w(x, y, z)$ are the components of displacement at a general point in Ω on the x , y , and z axes, respectively; $w(x, y)$ represents the transverse deflection and $\beta_x(x, y)$ and

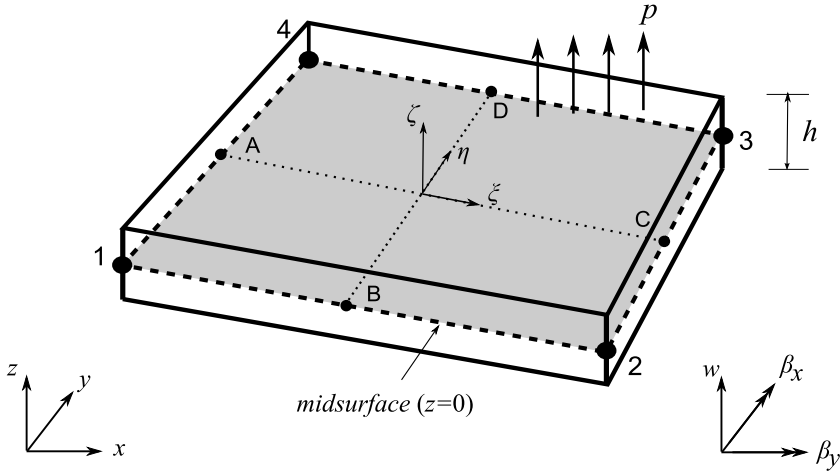


Figure 1. Quadrilateral shear deformable plate element.

$\beta_y(x, y)$ are the rotations in the x and y directions of the middle surface, respectively. The bending and shear strains for Mindlin–Reissner plate theory are given by

$$\boldsymbol{\kappa} = \begin{bmatrix} \beta_{x,x} \\ \beta_{y,y} \\ \beta_{x,y} + \beta_{y,x} \end{bmatrix}, \quad \boldsymbol{\gamma} = \begin{bmatrix} \beta_x + w_{,x} \\ \beta_y + w_{,y} \end{bmatrix}. \tag{2}$$

The total potential energy for a shear deformable plate subjected to in-plane prebuckling stresses ($\hat{\boldsymbol{\sigma}}_0$), in the absence of other external forces and neglecting terms with third and higher powers, can be written as

$$\begin{aligned} \Pi = & \frac{1}{2} \iiint_V \boldsymbol{\kappa}^T \mathbf{Q}_b \boldsymbol{\kappa} \, dx \, dy \, dz + \frac{1}{2} \iiint_V \boldsymbol{\gamma}^T \mathbf{Q}_s \boldsymbol{\gamma} \, dx \, dy \, dz + \iiint_V \sigma_{xx}^0 \varepsilon_{xx}^{NL} \, dx \, dy \, dz \\ & + \iiint_V \sigma_{yy}^0 \varepsilon_{yy}^{NL} \, dx \, dy \, dz + \iiint_V \sigma_{xy}^0 \varepsilon_{xy}^{NL} \, dx \, dy \, dz, \end{aligned} \tag{3}$$

where

$$\begin{Bmatrix} \varepsilon_{xx}^{NL} \\ \varepsilon_{yy}^{NL} \\ \varepsilon_{xy}^{NL} \end{Bmatrix} = \begin{Bmatrix} \frac{1}{2} ((u_{,x})^2 + (v_{,x})^2 + (w_{,x})^2) \\ \frac{1}{2} ((u_{,y})^2 + (v_{,y})^2 + (w_{,y})^2) \\ (u_{,x} u_{,y} + v_{,x} v_{,y} + w_{,x} w_{,y}) \end{Bmatrix}. \tag{4}$$

Combining (1)–(4) and integrating over the thickness (3), the total potential energy can be rewritten

$$\begin{aligned} \Pi = & \frac{1}{2} \iint_{\Omega} \boldsymbol{\kappa}^T \mathbf{D}_b \boldsymbol{\kappa} \, dx \, dy + \frac{1}{2} \iint_{\Omega} \boldsymbol{\gamma}^T \mathbf{D}_s \boldsymbol{\gamma} \, dx \, dy + \frac{1}{2} \iint_{\Omega} [w_{,x} \ w_{,y}] \hat{\boldsymbol{\sigma}}_0 \begin{Bmatrix} w_{,x} \\ w_{,y} \end{Bmatrix} h \, dx \, dy \\ & + \frac{1}{2} \iint_{\Omega} [\beta_{x,x} \ \beta_{x,y}] \hat{\boldsymbol{\sigma}}_0 \begin{Bmatrix} \beta_{x,x} \\ \beta_{x,y} \end{Bmatrix} \frac{h^3}{12} \, dx \, dy + \frac{1}{2} \iint_{\Omega} [\beta_{y,x} \ \beta_{y,y}] \hat{\boldsymbol{\sigma}}_0 \begin{Bmatrix} \beta_{y,x} \\ \beta_{y,y} \end{Bmatrix} \frac{h^3}{12} \, dx \, dy. \end{aligned} \tag{5}$$

The coefficient matrices in (3) are defined as

$$D_b = \frac{Eh^3}{12(1-\nu^2)} \begin{bmatrix} 1 & \nu & 0 \\ \nu & 1 & 0 \\ 0 & 0 & \frac{1}{2}(1-\nu) \end{bmatrix}, \quad D_s = \frac{k_s Eh}{2(1+\nu)} \begin{bmatrix} 1 & 0 \\ 0 & 1 \end{bmatrix}, \quad (6)$$

$$\hat{\sigma}_0 = \begin{bmatrix} \sigma_{xx}^0 & \sigma_{xy}^0 \\ \sigma_{yx}^0 & \sigma_{yy}^0 \end{bmatrix}, \quad (7)$$

where D_b is the bending stiffness matrix, D_s the shear stiffness matrix, E the Young's modulus, ν the Poisson ratio, and k_s the transverse shear correction factor (taken as $\frac{5}{6}$ in this work).

2.2. Finite element implementation (Q4). The problem domain Ω will be discretised into a finite number of quadrilateral isoparametric elements Ne :

$$\Omega \approx \Omega^h = \bigcup_{e=1}^{Ne} \Omega^e.$$

Using the shape functions of the quadrilateral element shown in Figure 1, lateral displacement and rotations can be expressed as

$$w = \sum_{i=1}^4 N_i w_i, \quad \beta_x = \sum_{i=1}^4 N_i \beta_{xi}, \quad \beta_y = \sum_{i=1}^4 N_i \beta_{yi}, \quad (8)$$

where w_i , β_{xi} , and β_{yi} denote nodal displacements and rotations and N_i the vector of bilinear shape functions. Using the approximation in (8) the following expansions can be written:

$$\kappa = B_b q, \quad \gamma = B_s q, \quad (9)$$

$$\begin{Bmatrix} w_{,x} \\ w_{,y} \end{Bmatrix} = G_b q, \quad \begin{Bmatrix} \beta_{x,x} \\ \beta_{x,y} \end{Bmatrix} = G_{s1} q, \quad \begin{Bmatrix} \beta_{y,x} \\ \beta_{y,y} \end{Bmatrix} = G_{s2} q, \quad (10)$$

where

$$B_{bi} = \begin{bmatrix} 0 & N_{i,x} & 0 \\ 0 & 0 & N_{i,y} \\ 0 & N_{i,y} & N_{i,x} \end{bmatrix}, \quad B_{si} = \begin{bmatrix} N_{i,x} & N_i & 0 \\ N_{i,y} & 0 & N_i \end{bmatrix}, \quad q_i = \begin{bmatrix} w_i \\ \beta_{xi} \\ \beta_{yi} \end{bmatrix}, \quad (11)$$

$$G_{bi} = \begin{bmatrix} N_{i,x} & 0 & 0 \\ N_{i,y} & 0 & 0 \end{bmatrix}, \quad G_{s1i} = \begin{bmatrix} 0 & N_{i,x} & 0 \\ 0 & N_{i,y} & 0 \end{bmatrix}, \quad G_{s2i} = \begin{bmatrix} 0 & 0 & N_{i,x} \\ 0 & 0 & N_{i,y} \end{bmatrix}. \quad (12)$$

Using (8)–(12), the stationary form of the total potential energy expression (3) can be expressed as

$$(K - \lambda K_G) q^m = 0, \quad m = 1, 2, \dots \text{ degrees of freedom}, \quad (13)$$

where K is the global stiffness matrix, K_G is the geometrical stiffness matrix, λ is a scalar by which the chosen in-plane loads must be multiplied in order to cause buckling, and vector q^m is the m -th buckling mode. The stiffness matrices in (13) can be explicitly written as

$$K = K_b + K_s,$$

that is,

$$\mathbf{K} = \int_{\Omega^e} \mathbf{B}_b^T \mathbf{D}_b \mathbf{B}_b d\Omega^e + \int_{\Omega^e} \mathbf{B}_s^T \mathbf{D}_s \mathbf{B}_s d\Omega^e \quad (14)$$

and $\mathbf{K}_G \mathbf{K}_{Gb} + \mathbf{K}_{Gs}$, with

$$\mathbf{K}_{Gb} = h \int_{\Omega^e} \mathbf{G}_b^T \hat{\boldsymbol{\sigma}}_0 \mathbf{G}_b d\Omega^e, \quad (15)$$

$$\mathbf{K}_{Gs} = \frac{h^3}{12} \int_{\Omega^e} \mathbf{G}_{s1}^T \hat{\boldsymbol{\sigma}}_0 \mathbf{G}_{s1} d\Omega^e + \frac{h^3}{12} \int_{\Omega^e} \mathbf{G}_{s2}^T \hat{\boldsymbol{\sigma}}_0 \mathbf{G}_{s2} d\Omega^e. \quad (16)$$

The shear contribution for the geometric stiffness matrix (\mathbf{K}_{Gs}) is negligible for thin plates, but its effect becomes more significant as the plate thickness increases. Most of the available literature dealing with buckling of cracked plates does not consider the effect of (16); therefore, in order to establish meaningful comparisons with the reported literature [Stahl and Keer 1972; Liu 2001; Purbolaksono and Aliabadi 2005] this term could be included or neglected in the numerical solution (in the present work, all examples considered neglect this term).

2.3. Shear locking. It is well known that the bilinear element described above exhibits shear locking as the plate thickness approaches the Kirchhoff limit. This is due to the fact that when using the bilinear interpolation for displacements and rotations the transverse shear strains cannot vanish at all points in the element when subjected to a constant bending moment. To overcome this deficiency, various remedies such as reduced integration have been proposed. In the present work, classical reduced integration and MITC (mixed interpolation of tensorial components) [Bathe and Dvorkin 1985] approaches will be used to eliminate shear locking.

In the classical approach, the shear part of the stiffness matrix, \mathbf{K}_s in (14), will be integrated using a 1×1 Gauss quadrature to avoid shear locking; this element will be referred to as Q4R.

In the approach proposed by [Bathe and Dvorkin 1985] displacement and rotations are interpolated as usual, but for the transverse shear strains, the covariant components measured in the natural coordinate system are interpolated. Following [Bathe and Dvorkin 1985] for the approximation of the shear strains, the second equation in (2) can be expressed as

$$\boldsymbol{\gamma} = \begin{bmatrix} \gamma_x \\ \gamma_y \end{bmatrix} = \mathbf{J}^{-1} \begin{bmatrix} \gamma_\xi \\ \gamma_\eta \end{bmatrix}, \quad (17)$$

with

$$\gamma_\xi = \frac{1}{2} [(1 - \eta)\gamma_\xi^B + (1 + \eta)\gamma_\xi^D], \quad (18)$$

$$\gamma_\eta = \frac{1}{2} [(1 - \xi)\gamma_\eta^A + (1 + \xi)\gamma_\eta^C], \quad (19)$$

where \mathbf{J} is the Jacobian matrix and γ_η^A , γ_ξ^B , γ_η^C , and γ_ξ^D are the (physical) shear strains at the midside points A , B , C , and D , shown in Figure 1 together with the global (x, y, z) and local (ξ, η, ζ) coordinate systems. Using (17) and (19) and following the description in [Gruttmann and Wagner 2004], the shear part of the stiffness matrix, \mathbf{K}_s in (14), can be rewritten as

$$\bar{\mathbf{B}}_{si} = \mathbf{J}^{-1} \begin{bmatrix} N_{i,\xi} & b_i^{11} N_{i,\xi} & b_i^{12} N_{i,\xi} \\ N_{i,\eta} & b_i^{21} N_{i,\eta} & b_i^{22} N_{i,\eta} \end{bmatrix}, \quad (20)$$

where

$$b_i^{11} = \xi_i x_{,\xi}^M, \quad b_i^{12} = \xi_i y_{,\xi}^M, \quad b_i^{21} = \eta_i x_{,\eta}^L, \quad b_i^{22} = \eta_i y_{,\eta}^L. \tag{21}$$

The coordinates of the unit square are $\xi_i \in \{-1, 1, 1, -1\}$, $\eta_i \in \{-1, -1, 1, 1\}$ and the allocation of the midside nodes to the corner nodes is given by $(i, M, L) \in \{(1, B, A); (2, B, C); (3, D, C); (4, D, A)\}$, see Figure 1. Using (20), now the shear part of the stiffness matrix (\mathbf{K}_s) can be computed using full integration (2×2 Gauss quadrature); this element will be referred to as MITC.

3. Curvature strain smoothing

Strain smoothing has appeared in the finite element literature [Liu et al. 2007a; Nguyen-Xuan et al. 2008b] as an attractive option to obtain increased accuracy at a lower computational cost, deal with mesh distortion, and avoid locking, among other advantages. The idea behind the method is to express the strain field as a spatial average of the compatible strains and use this “smoothed strain” to obtain the element stiffness matrix.

Curvature strain smoothing for plate bending was first proposed in [Wang and Chen 2004] in meshfree methods and in [Nguyen-Xuan et al. 2008b] in a finite element framework. Following the derivation in [Nguyen-Xuan et al. 2008b], the smoothed bending strains for Mindlin–Reissner plates are given as

$$\tilde{\boldsymbol{\kappa}} = \tilde{\mathbf{B}}_b^C \mathbf{q}, \tag{22}$$

and the corresponding smoothed element bending stiffness matrix is

$$\tilde{\mathbf{K}}_b = \int_{\Omega^e} (\tilde{\mathbf{B}}_b^C)^T \mathbf{D}_b \tilde{\mathbf{B}}_b^C d\Omega^e = \sum_{C=1}^{nc} (\tilde{\mathbf{B}}_b^C(\mathbf{x}_C))^T \mathbf{D}_b \tilde{\mathbf{B}}_b^C(\mathbf{x}_C) A_C, \tag{23}$$

where nc is the number of smoothing cells in the element. As described in [Nguyen-Xuan et al. 2008b], the integrands are constant over each smoothing cell domain (Ω_C^e) and the nonlocal curvature displacement matrix is given by

$$\tilde{\mathbf{B}}_{bi}^C(\mathbf{x}_C) = \frac{1}{A_C} \int_{\Gamma_C} \begin{pmatrix} 0 & N_i n_x & 0 \\ 0 & 0 & N_i n_y \\ 0 & N_i n_y & N_i n_x \end{pmatrix} d\Gamma_C. \tag{24}$$

This equation is evaluated using one Gauss point over each boundary cell segment Γ_C^m :

$$\tilde{\mathbf{B}}_{bi}^C(\mathbf{x}_C) = \frac{1}{A_C} \sum_{m=1}^{mt} \begin{pmatrix} 0 & N_i(\mathbf{x}_m^G) n_x(\mathbf{x}_m^G) & 0 \\ 0 & 0 & N_i(\mathbf{x}_m^G) n_y(\mathbf{x}_m^G) \\ 0 & N_i(\mathbf{x}_m^G) n_y(\mathbf{x}_m^G) & N_i(\mathbf{x}_m^G) n_x(\mathbf{x}_m^G) \end{pmatrix} l_m^C, \tag{25}$$

where \mathbf{x}_m^G is the Gauss point (midpoint of segment m), l_m^C is the length of segment m , and mt is the total number of segments. The expression in (25) already includes the product of the Jacobian of transformation for a 1D 2-node element ($l_m^C/2$) and the Gauss quadrature weight (2). Combining the curvature strain smoothing and the mixed interpolation of tensorial components gives the following expression for

the stiffness matrix of a Mindlin–Reissner plate:

$$\tilde{\mathbf{K}} = \tilde{\mathbf{K}}_b + \tilde{\mathbf{K}}_s, \tag{26}$$

$$\tilde{\mathbf{K}} = \sum_{C=1}^{nc} (\tilde{\mathbf{B}}_b^C(\mathbf{x}_C))^T \mathbf{D}_b \tilde{\mathbf{B}}_b^C(\mathbf{x}_C) A_C + \int_{\Omega^e} \bar{\mathbf{B}}_s^T \mathbf{D}_s \bar{\mathbf{B}}_s d\Omega^e. \tag{27}$$

As mentioned in [Nguyen-Xuan et al. 2008b], this element will be referred to as MISC*k* (mixed interpolation and smoothed curvatures) with $k \in \{1, 2, 3, 4\}$ representing the number of smoothing cells (nc). These elements were shown to pass the patch test and to be slightly more accurate than the MITC for regular meshes. The most promising feature was their improved performance for irregular meshes and coarse meshes and their lower computational cost.

3.1. Smoothing of bending geometric stiffness matrix. Following a similar approach as the one presented by [Wang and Chen 2004; Nguyen-Xuan et al. 2008b] and shown above, the bending part of the geometric stiffness matrix given in (15) can be written as

$$\tilde{\mathbf{K}}_{Gb} = h \int_{\Omega^e} (\tilde{\mathbf{G}}_b^C)^T \hat{\boldsymbol{\sigma}}_0 \tilde{\mathbf{G}}_b^C d\Omega^e = h \sum_{C=1}^{nc} (\tilde{\mathbf{G}}_b^C(\mathbf{x}_C))^T \hat{\boldsymbol{\sigma}}_0 \tilde{\mathbf{G}}_b^C(\mathbf{x}_C) A_C, \tag{28}$$

where

$$\tilde{\mathbf{G}}_{bi}^C(\mathbf{x}_C) = \frac{1}{A_C} \int_{\Gamma_C} \begin{pmatrix} N_i n_x & 0 & 0 \\ N_i n_y & 0 & 0 \end{pmatrix} d\Gamma_C. \tag{29}$$

Following the same numerical implementation used for (24), (29) will be evaluated using one Gauss point over each boundary cell segment Γ_C :

$$\tilde{\mathbf{G}}_{bi}^C(\mathbf{x}_C) = \frac{1}{A_C} \sum_{m=1}^{mt} \begin{pmatrix} N_i(\mathbf{x}_m^G) n_x(\mathbf{x}_m^G) & 0 & 0 \\ N_i(\mathbf{x}_m^G) n_y(\mathbf{x}_m^G) & 0 & 0 \end{pmatrix} I_m^C. \tag{30}$$

Using this expression in (28) corresponds to smoothing the higher-order bending terms given in (4). This case will be considered in the present work, in order to study the effect of smoothing higher-order terms within a shear deformable plate formulation. This element will be defined as MISC*k*_b (mixed interpolation and smoothed curvatures of global stiffness and geometric stiffness matrix). Similarly to MISC*k*, the number k in MISC*k*_b represents the number of smoothing cells in the element.

4. Extended finite element method for shear deformable plates

Following a similar enriched approximation for plate bending as presented in [Dolbow et al. 2000], deflection and rotations can be approximated as

$$\mathbf{w}^h(\mathbf{x}) = \sum_{i \in N^{\text{fem}}} N_i(\mathbf{x}) w_i + \sum_{j \in N^{\text{crack}}} N_j(\mathbf{x}) \bar{H}_j(\mathbf{x}) b_j^w + \sum_{k \in N^{\text{tip}}} N_k(\mathbf{x}) \left(\sum_{l=1}^4 \bar{G}_{lk}(r, \theta) c_{kl}^w \right), \tag{31}$$

$$\boldsymbol{\beta}^h(\mathbf{x}) = \sum_{i \in N^{\text{fem}}} N_i(\mathbf{x}) \beta_i + \sum_{j \in N^{\text{crack}}} N_j(\mathbf{x}) \bar{H}_j(\mathbf{x}) b_j^\beta + \sum_{k \in N^{\text{tip}}} N_k(\mathbf{x}) \left(\sum_{l=1}^4 \bar{F}_{lk}(r, \theta) c_{kl}^\beta \right), \tag{32}$$

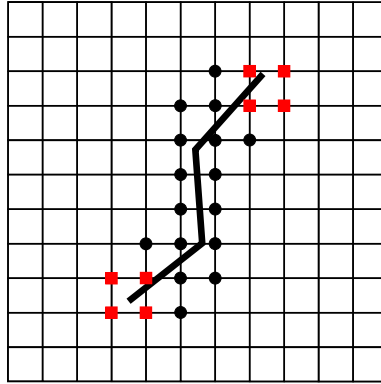


Figure 2. Crack on an uniform mesh of bilinear quadrilateral elements. Circle nodes are enriched by jump functions and square nodes by the asymptotic crack tip field.

where $N(\mathbf{x})$ denotes the standard bilinear shape functions, w_i and β_i the nodal unknowns associated with the continuous solution, b_j the nodal enriched degrees of freedom associated with the Heaviside function $\bar{H}_j(\mathbf{x})$, and c_{kl} the nodal enriched degrees of freedom associated with the elastic asymptotic crack tip functions $\bar{G}_{lk}(r, \theta)$ and $\bar{F}_{lk}(r, \theta)$. In (31) and (32) N^{fem} is the set of all nodes in the mesh, N^{crack} is the set of nodes whose shape function support is cut by the crack interior (circular nodes in Figure 2), and N^{tip} is the set of nodes whose shape function support is cut by the crack tip (square nodes in Figure 2).

4.1. Enrichment functions. The shifted enrichment functions in (31) and (32) are given by

$$\bar{H}_i(\mathbf{x}) = (H(\mathbf{x}) - H(\mathbf{x}_i)), \tag{33}$$

$$\bar{G}_{li}(\mathbf{x}) = (G_l(\mathbf{x}) - G_l(\mathbf{x}_i)), \quad \bar{F}_{li}(\mathbf{x}) = (F_l(\mathbf{x}) - F_l(\mathbf{x}_i)). \tag{34}$$

Shifting the enrichment functions is particularly useful because the influence of the enrichment on the displacement must vanish at the nodes for ease of applying boundary conditions.

The Heaviside enrichment function $H(\mathbf{x})$ in (33) is defined by

$$H(\mathbf{x}) = \begin{cases} +1 & \text{if the point is above the crack face,} \\ -1 & \text{if the point is below the crack face.} \end{cases} \tag{35}$$

Equation (35) is responsible for the description of the interior of the crack (jump in displacements).

The elastic crack tip enrichment functions in (34) are defined as (see [Dolbow et al. 2000; Bordas et al. 2009])

$$\{G_l(r, \theta)\} \equiv \left\{ r^{3/2} \sin\left(\frac{\theta}{2}\right), r^{3/2} \cos\left(\frac{\theta}{2}\right), r^{3/2} \sin\left(\frac{3\theta}{2}\right), r^{3/2} \cos\left(\frac{3\theta}{2}\right) \right\}, \tag{36}$$

$$\{F_l(r, \theta)\} \equiv \left\{ \sqrt{r} \sin\left(\frac{\theta}{2}\right), \sqrt{r} \cos\left(\frac{\theta}{2}\right), \sqrt{r} \sin\left(\frac{\theta}{2}\right) \sin(\theta), \sqrt{r} \cos\left(\frac{\theta}{2}\right) \sin(\theta) \right\}. \tag{37}$$

Here (r, θ) are polar coordinates with origin at the crack tip. These functions are not only responsible for closing the crack at the tip but they also introduce analytical information in the numerical approximation.

5. Smoothed extended finite element method

In [Bordas et al. 2009] it was shown how strain smoothing could be incorporated into XFEM formulations (including plate bending). In SmXFEM, smoothing must now be performed on discontinuous and nonpolynomial approximations. In the present case, curvature smoothing coupled with partition of unity enrichment can produce a plate element capable of cracking which is significantly more accurate than formerly proposed elements [Bordas et al. 2009].

5.1. Summary of plate formulations. As outlined in previous sections, four plate elements (enriched or standard) are considered in the present work:

- Q4R: This plate element uses the basic FE formulation for Mindlin–Reissner plate theory. It uses the standard gradient operators (plain shape function derivatives) for both bending and shear parts, and in order to avoid shear locking the shear part of the stiffness matrix, \mathbf{K}_s in (14), will be integrated using a 1×1 Gauss quadrature.
- MITC: This element interpolates the out-of-plane shear stresses using collocation points at the element boundaries. It uses the standard gradient operators for the bending part (\mathbf{K}_b), and the mixed interpolation of tensorial components [Bathe and Dvorkin 1985] for the shear part (\mathbf{K}_s) of the stiffness matrix, (20).
- MISCk: This element, first introduced in [Nguyen-Xuan et al. 2008b], uses the curvature strain smoothing operator for the bending part given by (25), and the mixed interpolation of tensorial components [Bathe and Dvorkin 1985] for the shear part of the stiffness matrix given by (20), leading to the expression in (27).
- MISCk_b: This element is similar to MISCk but instead of using the standard operator for the bending part of the geometric matrix given by (15), it uses a smoothing operator for the higher-order terms given in (4). In other words, it uses the expression in (27) for the stiffness matrix (\mathbf{K}) and the expression in (30) for the bending part of the geometric stiffness matrix (\mathbf{K}_{Gb}).

5.2. Strain smoothing in XFEM plate bending. In this subsection, detailed description of the SmXFEM implementation for the buckling analysis of cracked Mindlin–Reissner plates is provided. For the sake of simplicity, only the expressions for the enriched MISCk element will be shown here. Enriched smoothed bending strain and enriched shear strain can be written as

$$\tilde{\kappa}^h = \sum_{i \in N^{fem}} \tilde{\mathbf{B}}_{b_{fem}^i}^C \mathbf{q}_i + \sum_{j \in N^{crack}} \tilde{\mathbf{B}}_{b_{crack}^j}^C \mathbf{b}_j + \sum_{k \in N^{tip}} \tilde{\mathbf{B}}_{b_{tip}^k}^C \mathbf{c}_k, \tag{38}$$

$$\boldsymbol{\gamma}^h = \sum_{i \in N^{fem}} \tilde{\mathbf{B}}_{s_{fem}^i} \mathbf{q}_i + \sum_{j \in N^{crack}} \tilde{\mathbf{B}}_{s_{crack}^j} \mathbf{b}_j + \sum_{k \in N^{tip}} \tilde{\mathbf{B}}_{s_{tip}^k} \mathbf{c}_k. \tag{39}$$

The enriched gradient operators in (38) and (39) can be explicitly written as

$$\tilde{\mathbf{B}}_{b_{crack}^j}^C(\mathbf{x}_C) = \frac{1}{A_C} \sum_{m=1}^{mt} \begin{pmatrix} 0 & N_j(\mathbf{x}_m^G) \bar{H}_j(\mathbf{x}_m^G) n_x(\mathbf{x}_m^G) & 0 \\ 0 & 0 & N_j(\mathbf{x}_m^G) \bar{H}_j(\mathbf{x}_m^G) n_y(\mathbf{x}_m^G) \\ 0 & N_j(\mathbf{x}_m^G) \bar{H}_j(\mathbf{x}_m^G) n_y(\mathbf{x}_m^G) & N_j(\mathbf{x}_m^G) \bar{H}_j(\mathbf{x}_m^G) n_x(\mathbf{x}_m^G) \end{pmatrix} \mathbf{l}_m^C, \tag{40}$$

$$\tilde{\mathbf{B}}_{b_{tip}^C}(\mathbf{x}_C)|_{l=1,2,3,4} = \frac{1}{A_C} \sum_{m=1}^{mt} \begin{pmatrix} 0 & N_k(\mathbf{x}_m^G) \bar{F}_{lk}(\mathbf{x}_m^G) n_x(\mathbf{x}_m^G) & 0 \\ 0 & 0 & N_k(\mathbf{x}_m^G) \bar{F}_{lk}(\mathbf{x}_m^G) n_y(\mathbf{x}_m^G) \\ 0 & N_k(\mathbf{x}_m^G) \bar{F}_{lk}(\mathbf{x}_m^G) n_y(\mathbf{x}_m^G) & N_k(\mathbf{x}_m^G) \bar{F}_{lk}(\mathbf{x}_m^G) n_x(\mathbf{x}_m^G) \end{pmatrix} l_m^C \quad (41)$$

and

$$\bar{\mathbf{B}}_{s_{crack}j} = \mathbf{J}^{-1} \begin{bmatrix} [N_j(\mathbf{x}) \bar{H}_j(\mathbf{x})]_{,\xi} & b_j^{11} [N_j(\mathbf{x}) \bar{H}_j(\mathbf{x})]_{,\xi} & b_j^{12} [N_j(\mathbf{x}) \bar{H}_j(\mathbf{x})]_{,\xi} \\ [N_j(\mathbf{x}) \bar{H}_j(\mathbf{x})]_{,\eta} & b_j^{21} [N_j(\mathbf{x}) \bar{H}_j(\mathbf{x})]_{,\eta} & b_j^{22} [N_j(\mathbf{x}) \bar{H}_j(\mathbf{x})]_{,\eta} \end{bmatrix}, \quad (42)$$

$$\bar{\mathbf{B}}_{s_{tip}^k}|_{l=1,2,3,4} = \mathbf{J}^{-1} \begin{bmatrix} [N_k(\mathbf{x}) \bar{G}_{lk}(\mathbf{x})]_{,\xi} & b_i^{11} [N_k(\mathbf{x}) \bar{F}_{lk}(\mathbf{x})]_{,\xi} & b_i^{12} [N_k(\mathbf{x}) \bar{F}_{lk}(\mathbf{x})]_{,\xi} \\ [N_k(\mathbf{x}) \bar{G}_{lk}(\mathbf{x})]_{,\eta} & b_i^{21} [N_k(\mathbf{x}) \bar{F}_{lk}(\mathbf{x})]_{,\eta} & b_i^{22} [N_k(\mathbf{x}) \bar{F}_{lk}(\mathbf{x})]_{,\eta} \end{bmatrix}. \quad (43)$$

Similarly, for the bending and shear part of the geometric stiffness, the enriched gradient operators can be expressed as

$$\mathbf{G}_{b_{crack}j} = \begin{bmatrix} [N_j(\mathbf{x}) \bar{H}_j(\mathbf{x})]_{,x} & 0 & 0 \\ [N_j(\mathbf{x}) \bar{H}_j(\mathbf{x})]_{,y} & 0 & 0 \end{bmatrix}, \quad \mathbf{G}_{b_{tip}^k}|_{l=1,2,3,4} = \begin{bmatrix} [N_k(\mathbf{x}) \bar{G}_{lk}(\mathbf{x})]_{,x} & 0 & 0 \\ [N_k(\mathbf{x}) \bar{G}_{lk}(\mathbf{x})]_{,y} & 0 & 0 \end{bmatrix}, \quad (44)$$

$$\mathbf{G}_{s1_{crack}j} = \begin{bmatrix} 0 & [N_j(\mathbf{x}) \bar{H}_j(\mathbf{x})]_{,x} & 0 \\ 0 & [N_j(\mathbf{x}) \bar{H}_j(\mathbf{x})]_{,y} & 0 \end{bmatrix}, \quad \mathbf{G}_{s1_{tip}^k}|_{l=1,2,3,4} = \begin{bmatrix} 0 & [N_k(\mathbf{x}) \bar{F}_{lk}(\mathbf{x})]_{,x} & 0 \\ 0 & [N_k(\mathbf{x}) \bar{F}_{lk}(\mathbf{x})]_{,y} & 0 \end{bmatrix}, \quad (45)$$

$$\mathbf{G}_{s2_{crack}j} = \begin{bmatrix} 0 & 0 & [N_j(\mathbf{x}) \bar{H}_j(\mathbf{x})]_{,x} \\ 0 & 0 & [N_j(\mathbf{x}) \bar{H}_j(\mathbf{x})]_{,y} \end{bmatrix}, \quad \mathbf{G}_{s2_{tip}^k}|_{l=1,2,3,4} = \begin{bmatrix} 0 & 0 & [N_k(\mathbf{x}) \bar{F}_{lk}(\mathbf{x})]_{,x} \\ 0 & 0 & [N_k(\mathbf{x}) \bar{F}_{lk}(\mathbf{x})]_{,y} \end{bmatrix}. \quad (46)$$

5.3. Integration. As mentioned, the integrations of the discretised terms presented in the previous sections are done using Gauss quadrature. In the present work boundary and domain integrals are evaluated for the MISCK and MISCK_b elements (the smoothed terms are evaluated using surface integrals, whereas the nonsmooth are obtained using domain integration) and only domain integrals for the classical Q4R and MITC elements.

The standard (nonenriched) domain integration uses 2×2 Gauss quadrature as it evaluates the bilinear shape functions sufficiently. The only exception to the standard (nonenriched) domain integration is with the shear part of the stiffness matrix, \mathbf{K}_s in (14), which uses 1×1 Gauss quadrature.

For standard surface integration, terms in (25) and (30), two subcells with one Gauss point per boundary are used, as recommended in [Nguyen-Xuan et al. 2008b]; in this way computational efficiency and numerical stability are guaranteed. This implies that MISC2 and MISC2_b are the specific smoothed elements used in the present work.

For elements that are enriched the integration has to be adapted, so that the weak form on both sides of the crack contributes the correct enriched terms. The most common approach, which is also implemented here, is to subtriangulate the element (for example, Delaunay triangulation) in a way that the triangle edges conform with the discontinuity.

In the case of enriched elements using domain integration the following integration rules are used:

- Tip-blending elements: 16 Gauss points for the total element.
- Split-blending elements: 2 Gauss points for the total element.
- Split-tip-blending elements: 4 Gauss points for each triangular subelement.
- Split elements: 3 Gauss points for each triangular subelement.
- Tip elements: 13 Gauss points for each triangular subelement.

In the case of enriched elements using surface integration (smoothed enriched elements) the following integration rules are used:

- Tip-blending elements: 8 subcells with 1 Gauss points per edge.
- Split-blending elements: 2 subcells with 1 Gauss points per edge.
- Split-tip-blending elements: 4 subelements, each with 4 subcells with 1 Gauss points per edge.
- Split elements: 4 subelements, each with 2 subcells with 1 Gauss points per edge.
- Tip elements: 4 subelements, each with 8 subcells with 1 Gauss points per edge.

As in standard XFEM, there are 6 different types of elements:

- Tip elements are elements that contain the crack tip. All nodes belonging to a tip element are enriched with the near-tip fields ($\bar{G}_I(\mathbf{x})$ and $\bar{F}_I(\mathbf{x})$).
- Split elements are elements completely cut by the crack. Their nodes are enriched with the discontinuous function $\bar{H}(\mathbf{x})$.
- Tip-blending elements are elements neighbouring tip elements. They are such that some of their nodes are enriched with the near-tip fields ($\bar{G}_I(\mathbf{x})$ and $\bar{F}_I(\mathbf{x})$) and others are not enriched at all.
- Split-blending elements are elements neighbouring split elements. They are such that some of their nodes are enriched with the discontinuous function, $\bar{H}(\mathbf{x})$, and others are not enriched at all.
- Split-tip-blending elements are elements completely cut by the crack and neighbouring tip elements. They are such that all of their nodes are enriched with the discontinuous function, $\bar{H}(\mathbf{x})$, and some of their nodes are enriched with the near-tip fields ($\bar{G}_I(\mathbf{x})$ and $\bar{F}_I(\mathbf{x})$).
- Standard elements are elements that are in neither of the above categories. None of their nodes are enriched.

6. Numerical examples

In this section the formulation presented in the previous paragraphs is now applied to determine the normalised buckling coefficients for rectangular plates with different thicknesses (h/a), crack sizes (c/a), and boundary conditions. The plates have Young's modulus E , Poisson's ratio $\nu = 0.3$, length a (sides), and width b (ends). The compressive stress is applied in the longitudinal direction; see [Figure 3](#). The results are compared with available analytical and numerical solutions when available. Due to the crack orientation considered in all examples ([Figure 3](#)) traction free boundary conditions (no contact between crack faces) can be assumed in all cases.

Normalised results are obtained using the classical plate buckling coefficient (K):

$$K = \frac{b^2}{\pi^2 D} \sigma_{\text{cr}} = \frac{12(1 - \nu^2)b^2}{\pi^2 E h^3} \lambda \sigma. \quad (47)$$

Plate boundary conditions are defined as follows:

$$\text{Simply supported: } w = 0, \quad \beta_t = 0,$$

$$\text{Clamped: } w = 0, \quad \beta_n = 0, \quad \beta_t = 0,$$

where n denotes normal and t tangential directions to the plate boundary.

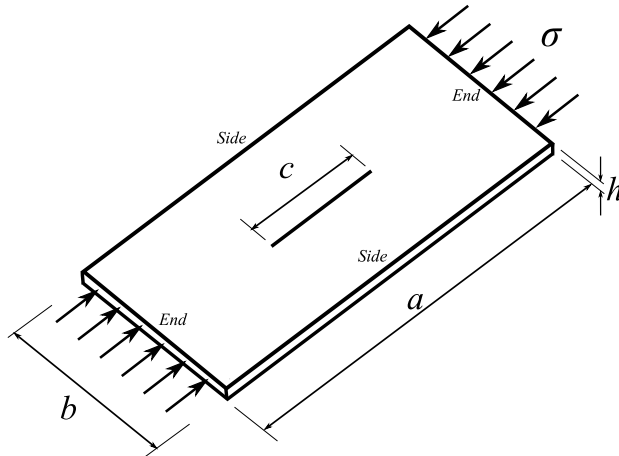


Figure 3. Centre crack plate geometry.

6.1. Buckling of simply supported plate (convergence). The first problem to be considered involves simply supported thin and thick square plates with no crack ($c/a = 0$). This example will illustrate the convergence performance of the recently developed MISC2 [Nguyen-Xuan et al. 2008b] and MISC2_b elements within the linear buckling problem (eigenvalue problem).

Six different uniform element distributions are considered in the convergence study (as shown in Tables 1 and 2). An analytical solution for linear buckling of Mindlin–Reissner plates was recently introduced

Mesh density	Q4R	MITC	MISC2	MISC2_b
11 × 11	4.0715 (1.79%)	4.0437 (1.09%)	4.0320 (0.80%)	4.0389 (0.97%)
15 × 15	4.0371 (0.93%)	4.0223 (0.56%)	4.0161 (0.40%)	4.0198 (0.49%)
19 × 19	4.0222 (0.55%)	4.013 (0.32%)	4.0092 (0.23%)	4.0115 (0.29%)
23 × 23	4.0144 (0.36%)	4.0082 (0.21%)	4.0055 (0.14%)	4.0071 (0.18%)
27 × 27	4.0098 (0.25%)	4.0053 (0.13%)	4.0034 (0.09%)	4.0045 (0.11%)
31 × 31	4.0069 (0.17%)	4.0035 (0.09%)	4.0020 (0.05%)	4.0029 (0.07%)

Table 1. Convergence of simply supported square plate with thickness ratio $h/a = 0.01$ (thin plate analytical solution $K = 4.000$).

Mesh density	Q4R	MITC	MISC2	MISC2_b
11 × 11	3.3127 (1.50%)	3.2943 (0.94%)	3.2865 (0.70%)	3.2922 (0.87%)
15 × 15	3.2899 (0.80%)	3.2801 (0.50%)	3.2760 (0.38%)	3.2790 (0.47%)
19 × 19	3.2800 (0.50%)	3.2739 (0.31%)	3.2713 (0.23%)	3.2732 (0.29%)
23 × 23	3.2748 (0.34%)	3.2707 (0.21%)	3.2689 (0.16%)	3.2702 (0.20%)
27 × 27	3.2718 (0.25%)	3.2688 (0.16%)	3.2675 (0.12%)	3.2684 (0.14%)
31 × 31	3.2698 (0.19%)	3.2676 (0.12%)	3.2666 (0.09%)	3.2673 (0.11%)

Table 2. Convergence of simply supported square plate with thickness ratio $h/a = 0.2$ (thick plate analytical solution $K = 3.2922$ [Hosseini-Hashemi et al. 2008]).

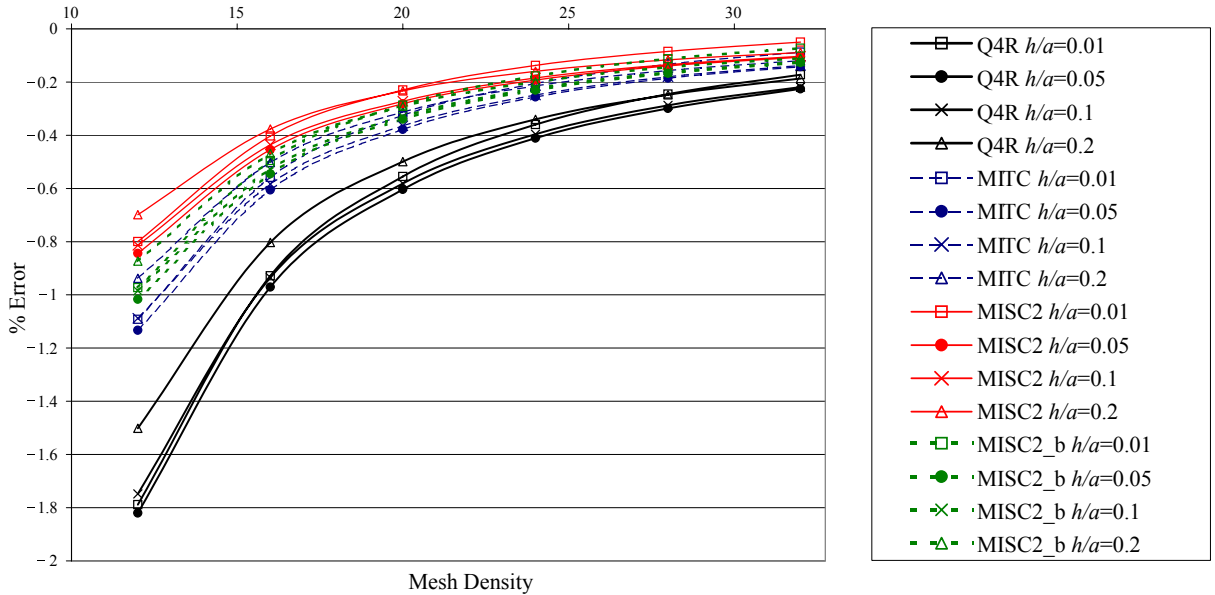


Figure 4. Convergence of normalised buckling coefficient for simply supported square ($a/b = 1$) plates ($c/a = 0$).

in [Hosseini-Hashemi et al. 2008] for a wide range of plate thicknesses that covers both thin and thick plates. Figure 4 presents an error comparison for each plate thickness ($h/a = 0.01, 0.05, 0.1, 0.2$) of all the elements considered in the present work. Additionally, Tables 1 and 2 present detailed results for only thin ($h/a = 0.01$) and very thick plates ($h/a = 0.2$), respectively.

As mentioned, the shear contribution for the geometric stiffness matrix (\mathbf{K}_{G_s}) is neglected in all cases in order to establish meaningful comparisons with the available analytical results [Stahl and Keer 1972; Liu 2001; Purbolaksono and Aliabadi 2005; Hosseini-Hashemi et al. 2008]. As can be seen from Figure 4, all results agree well with the analytical solution, with less than 2% difference for even the less refined mesh. The largest errors are obtained using the classical Q4R element while the smallest errors are obtained with the MISC2 element (always less than 1% error for even the less refined case). The MITC results are better than for the classical Q4R element but less accurate than the MISC2 and MISC2_b. Finally, it is possible to see from Figure 4 that the smoothed buckling element (MISC2_b) gives improved results over the MITC element but not better than the MISC2 element, implying that smoothing the higher powers of deformation given in (4) does not improve the element performance for regular meshes (not distorted).

Figure 5 shows the buckling modes for the coarsest mesh (11×11) used in the present example. The classical 1, 2, and 3 half ways expected for modes 1, 2, and 3 are clear in Figure 5.

6.2. Sensitivity to mesh distortion of uncracked plates. This second example will consider the effect of mesh distortion on the recently developed MISC2 [Nguyen-Xuan et al. 2008b] and MISC2_b elements within the linear buckling problem (eigenvalue problem). To study the effect of mesh distortion on the results, interior nodes are moved by an irregularity factor s . The coordinates of interior nodes are

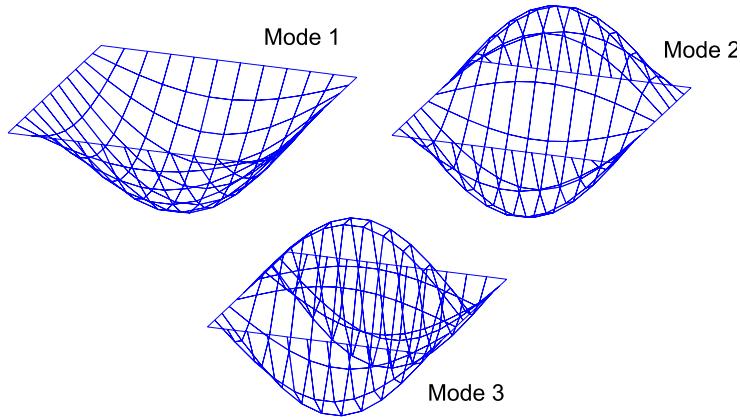


Figure 5. Buckling modes for simply supported square ($a/b = 1$) plate ($c/a = 0$).

obtained by the expressions [Liu et al. 2007a]

$$x' = x + sr_c \Delta x, \quad y' = y + sr_c \Delta y,$$

where r_c is a randomly generated number between -1.0 and 1.0 , $s \in [0, 0.4]$ is used to control the degree of element distortion, and Δx and Δy are initial regular element sizes in the x and y directions, respectively.

Thin ($h/a = 0.01$) and thick ($h/a = 0.1$) simply supported square plates ($a/b = 1$) with no crack ($c/a = 0$) will be considered. The less refined mesh of the previous example (11×11 elements) will be used in all cases (see Figure 6).

Tables 3 and 4 provide the buckling coefficients for thin ($h/a = 0.01$) and thick plates ($h/a = 0.1$), respectively, and Figure 7 plots the normalised values for both cases. In the case of thin plates, the classical Q4R shows the largest errors while the newly presented MISC2_b (with smoothed bending part of the geometric stiffness matrix) provides the best results. A similar behaviour occurs for thick plates but with much less detrimental effects for the classical Q4R. This dependency of mesh distortion on plate thickness has been shown in previous works [Nguyen-Xuan et al. 2008b].

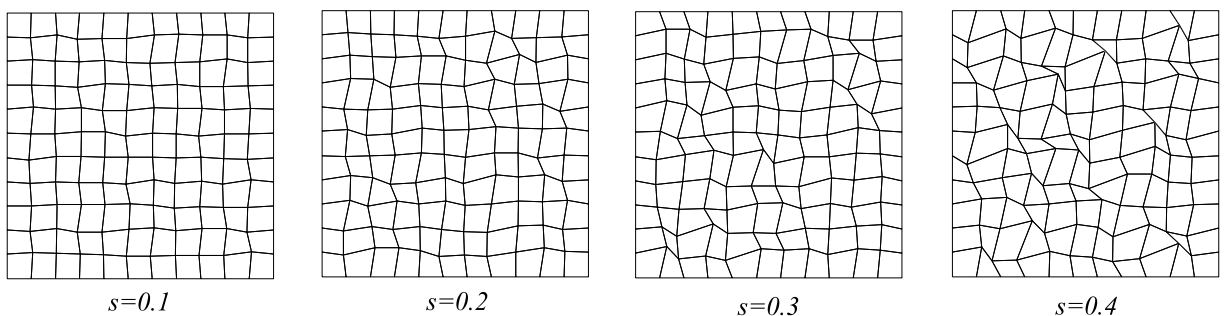


Figure 6. Effect of mesh distortion parameter in square plate with 11×11 elements.

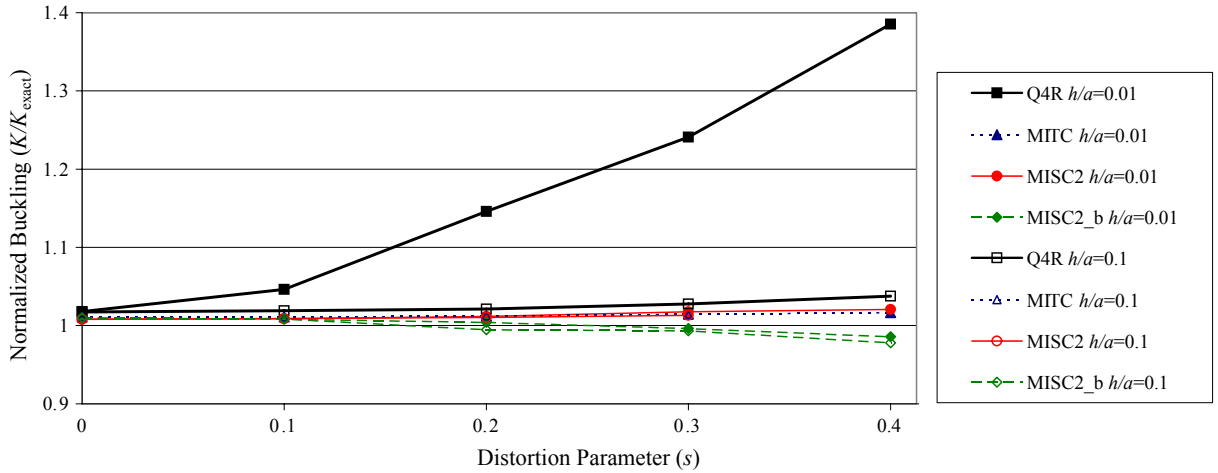


Figure 7. Influence of mesh distortion for buckling coefficient of simply supported square thin and thick plates.

From results in Tables 3 and 4 it is clear that although results for the smoothed buckling element (MISC2_b) give results that are not as accurate as the MISC2 element for regular meshes (no distortion), smoothing the higher powers of deformation given in (4) does improve the element performance for irregular meshes.

Mesh distortion	Q4R	MITC	MISC2	MISC2_b
0.0	4.0715 (1.79%)	4.0437 (1.09%)	4.0320 (0.80%)	4.0389 (0.97%)
0.1	4.1853 (4.63%)	4.0453 (1.13%)	4.0353 (0.88%)	4.0333 (0.83%)
0.2	4.5838 (14.6%)	4.0478 (1.19%)	4.0467 (1.17%)	4.0170 (0.43%)
0.3	4.9639 (24.1%)	4.0594 (1.48%)	4.0708 (1.77%)	3.9854 (0.37%)
0.4	5.5411 (38.5%)	4.0666 (1.66%)	4.0825 (2.06%)	3.9428 (1.43%)

Table 3. Effect of mesh distortion for simply supported square plate with thickness ratio $h/a = 0.01$ (thin plate analytical solution $K = 4.000$).

Mesh distortion	Q4R	MITC	MISC2	MISC2_b
0.0	3.8526 (1.75%)	3.8276 (1.09%)	3.8172 (0.81%)	3.8237 (0.99%)
0.1	3.8585 (1.90%)	3.8291 (1.13%)	3.8203 (0.89%)	3.8183 (0.84%)
0.2	3.8665 (2.12%)	3.8342 (1.26%)	3.8259 (1.04%)	3.7663 (0.53%)
0.3	3.8911 (2.76%)	3.8382 (1.37%)	3.8359 (1.31%)	3.7616 (0.65%)
0.4	3.9291 (3.77%)	–	–	3.7029 (2.20%)

Table 4. Effect of mesh distortion for simply supported square plate with thickness ratio $h/a = 0.1$ (thick plate analytical solution $K = 3.7864$ [Hosseini-Hashemi et al. 2008]).

6.3. Sensitivity to mesh distortion of plates with a longitudinal centre crack. This example extends on the previous example by including a longitudinal centre crack in the distorted mesh. Again, the same mesh density of the previous example will be used to obtain buckling coefficients of thin ($h/a = 0.01$) and thick ($h/a = 0.1$) simply supported square plates ($a/b = 1$) with a longitudinal centre crack ($c/a = 0.2$).

Tables 5 and 6 provide the buckling coefficients for thin ($h/a = 0.01$) and thick plates ($h/a = 0.1$), respectively; Figure 8 plots the normalised values for both cases. Table 5 shows why the classical Q4R is not used in XFEM plate formulations as it exhibits locking when modelling thin cracked plates (at least 50% error for regular meshes). The relatively large errors exhibited by other elements ($\sim 6\%$) is due to the coarse mesh size (11×11 elements) as will be shown in next examples.

6.4. Rectangular plate with a longitudinal centre crack. This example considers simply supported square and rectangular plates of different thickness ($h/a = 0.01, 0.1, 0.2$) with longitudinal centre cracks, as shown in Figure 3. All results were obtained with uniform meshes of 31×31 and 19×38 elements for the square and rectangular plates, respectively.

Figure 9 shows results for the square ($a/b = 1$) plates with Q4R-MITC and MISC2-MISC2_b elements, respectively. The classical Q4R element exhibits locking when modelling thin cracked plates ($h/a = 0.01$), and therefore are not shown in Figure 9. This is because when enriched elements are present in the model, a higher quadrature than 1×1 must be used (as mentioned in Section 5.3), leading to inaccurate results in the thin plate limit. All other elements exhibit an excellent performance for both thin and thick plates.

Mesh distortion	Q4R	MITC	MISC2	MISC2_b
0.0	5.8248 (52.2%)	4.0229 (5.15%)	4.0325 (5.40%)	4.0394 (5.58%)
0.1	6.1392 (60.5%)	4.0274 (5.27%)	4.0381 (5.55%)	4.0356 (5.48%)
0.2	6.5515 (71.2%)	4.0286 (5.30%)	4.0477 (5.80%)	3.9894 (4.27%)
0.3	7.2942 (90.7%)	4.0310 (5.36%)	4.0889 (6.87%)	3.9872 (4.21%)
0.4	–	–	–	3.9568 (3.42%)

Table 5. Effect of mesh distortion for simply supported square plate with thickness ratio $h/a = 0.01$ and longitudinal centre crack $c/a = 0.2$ (thin plate exact solution $K = 3.8259$ [Stahl and Keer 1972]).

Mesh distortion	Q4R	MITC	MISC2	MISC2_b
0.0	3.8235 (8.05%)	3.6606 (3.44%)	3.8170 (7.86%)	3.8236 (8.05%)
0.1	3.8158 (7.83%)	3.6569 (3.34%)	3.8185 (7.90%)	3.8142 (7.78%)
0.2	3.7931 (7.19%)	3.6497 (3.14%)	3.8256 (8.11%)	3.8003 (7.39%)
0.3	3.8800 (9.64%)	3.6931 (4.36%)	3.8474 (8.72%)	3.7538 (6.08%)
0.4	3.9557 (11.8%)	3.7160 (5.08%)	3.8553 (8.94%)	3.6420 (2.92%)

Table 6. Effect of mesh distortion for simply supported square plate with thickness ratio $h/a = 0.1$ and longitudinal centre crack $c/a = 0.2$ (thick plate solution $K = 3.53879$ [Liu 2001]).

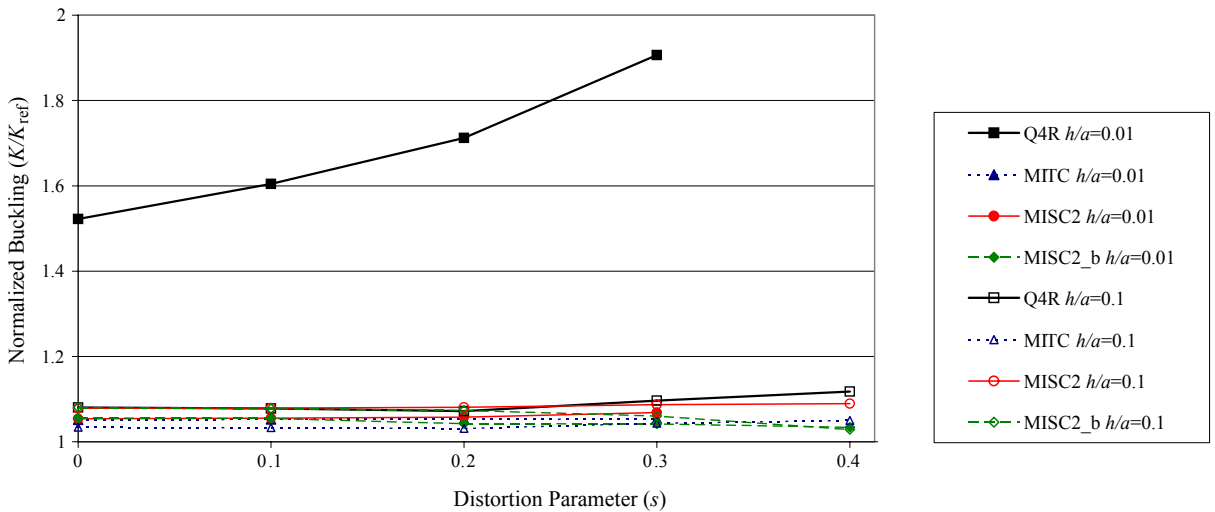


Figure 8. Influence of mesh distortion for buckling coefficient of simply supported square centre cracked ($c/a = 0.2$) thin and thick plates.

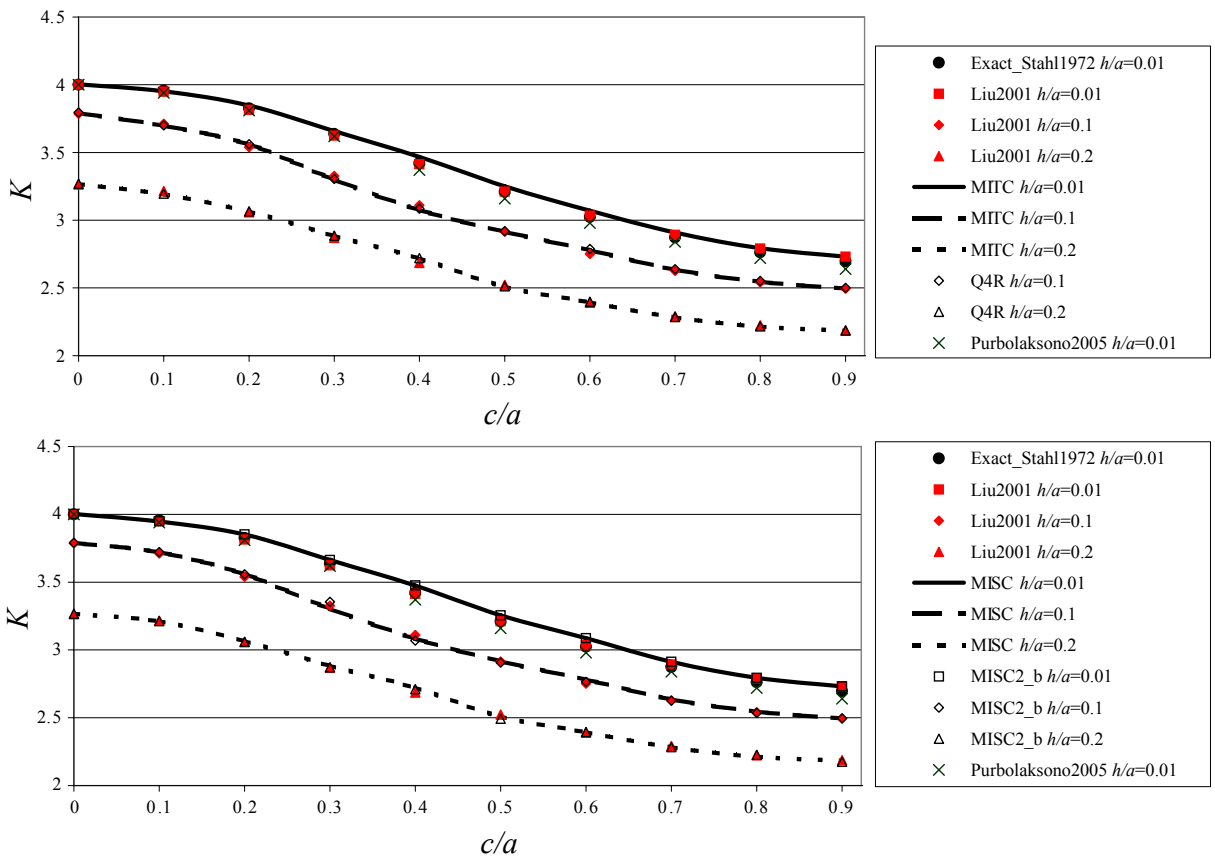


Figure 9. Buckling coefficients for square ($a/b = 1$) centre cracked plates. Top: Q4R and MITC. Bottom: MISC2 and MISC2_b.

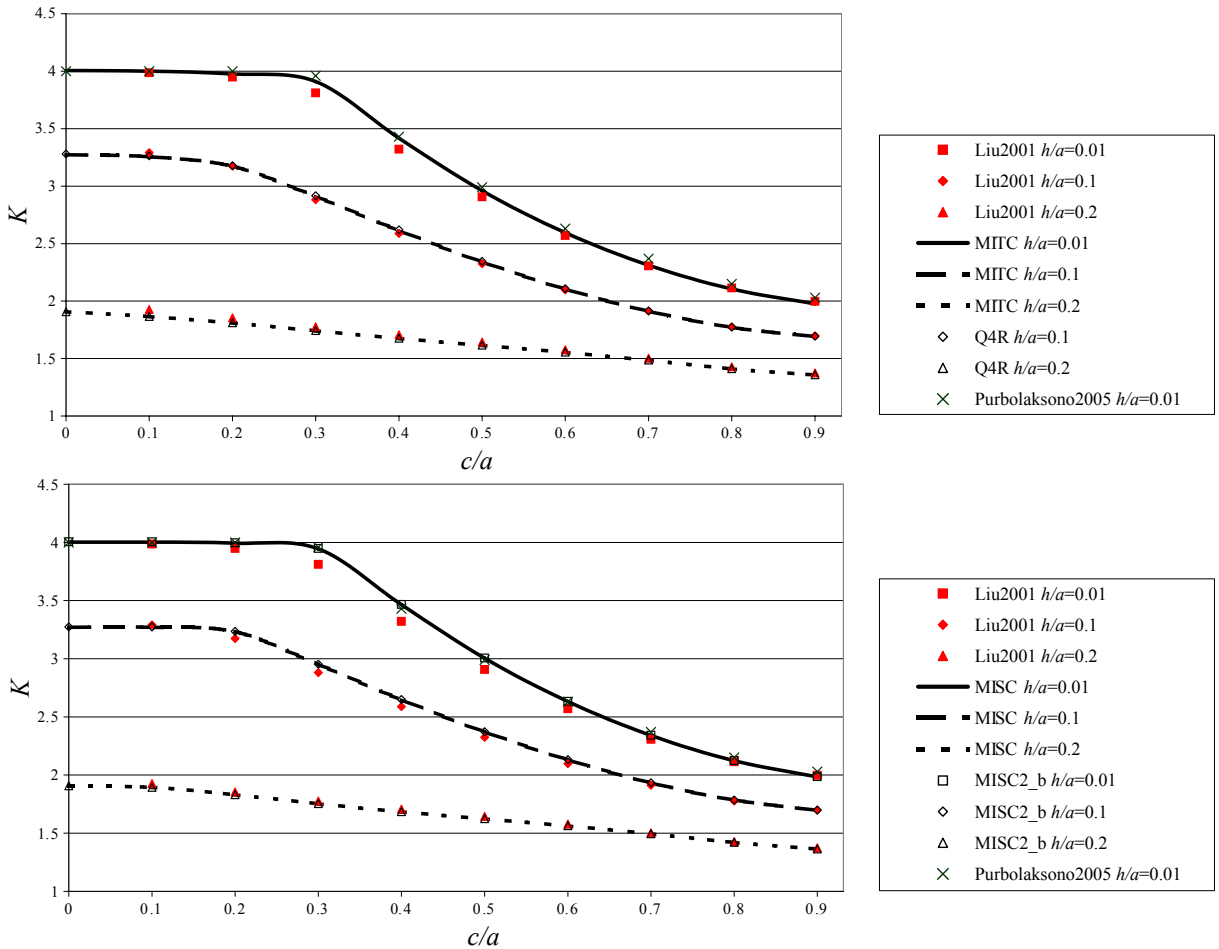


Figure 10. Buckling coefficients for rectangular ($a/b = 2$) centre cracked plates. Top: Q4R and MITC. Bottom: MISC2 and MISC2_b.

Figure 10 shows results for rectangular ($a/b = 2$) plates with Q4R-MITC and MISC2-MISC2_b elements, respectively. Again, results with the classical Q4R element are excluded for thin cracked plates ($h/a = 0.01$), due to locking.

As shown in Figures 9 and 10, an increase in crack length and thickness leads to a decrease on the critical buckling load. The 3 plate thicknesses ($h/a = 0.01, 0.1, 0.2$) and 10 crack sizes considered ($c/a = 0.0, 0.1, 0.2, 0.3, 0.4, 0.5, 0.6, 0.7, 0.8, 0.9$) give a clear picture of the behaviour of cracked thin and thick plates. In all cases results converge to the noncracked solution of thin and thick plates presented in the previous example.

In all cases good agreement is obtained with reported results (approximately 2% difference). The largest discrepancy ($\sim 3\%$) between reported solutions occurs for short-medium crack sizes ($a/c = 0.2, 0.3, 0.4, 0.5$) in rectangular plates (Figure 10). In this area the present results agree more with the results in [Purbolaksono and Aliabadi 2005] than with [Liu 2001], particularly for the MISC2 and MISC2_b elements.

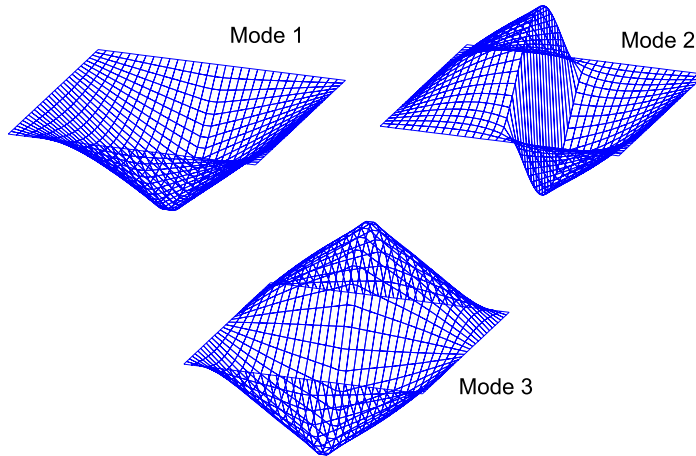


Figure 11. Buckling modes for simply supported centre cracked ($c/a = 0.9$) square plate ($a/b = 1$).

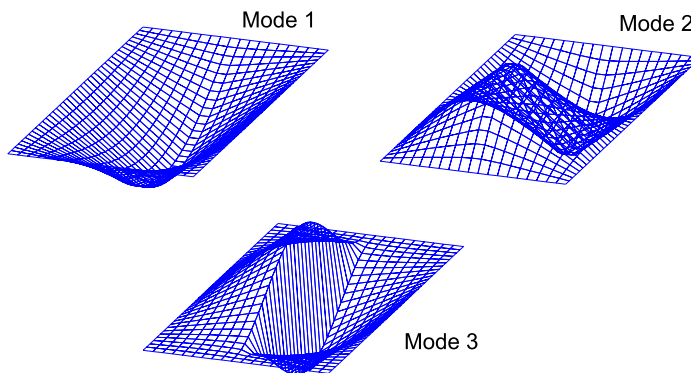


Figure 12. Buckling modes for simply supported centre cracked ($c/a = 0.9$) rectangular plate ($a/b = 2$).

Buckling modes for square and rectangular thin plates ($h/a = 0.01$) with the largest crack size ($a/c = 0.9$) are given in Figures 11 and 12, respectively. It is clear, by comparing Figures 5 and 11 that buckling modes change with the presence of the crack, in this case by adding a new mode (mode 2 in Figure 11) that replaces the classical second mode of 2 half waves (now mode 3 in Figure 11). Similarly, in the case of rectangular plates, instead of the classical 2 half waves for mode 1, now the presence of the crack leads to only 1 half waves mode (mode 1 in Figure 12).

6.5. Rectangular plate with a longitudinal edge crack. In this example, simply supported rectangular ($a/b = 2$) thin and thick plates with a transverse edge crack as shown in Figure 13 are analysed. Buckling coefficients for Q4R (except for the thin plate case $h/a = 0.01$) and MITC elements are given with respect to the normalised crack size in the top part of Figure 14. Similarly, the bottom part of the same figure shows buckling coefficients for MISC2 and MISC2_b elements. All results were obtained with an uniform mesh of 19×38 elements.

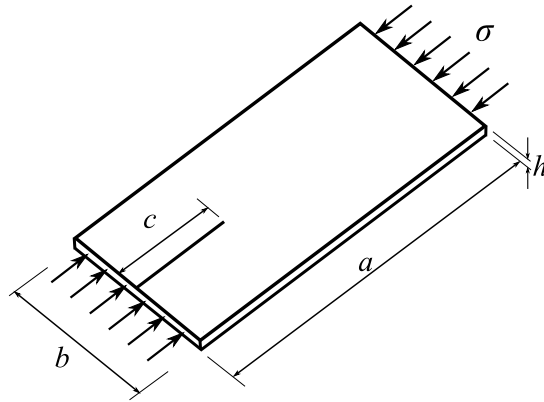


Figure 13. Edge crack plate geometry.

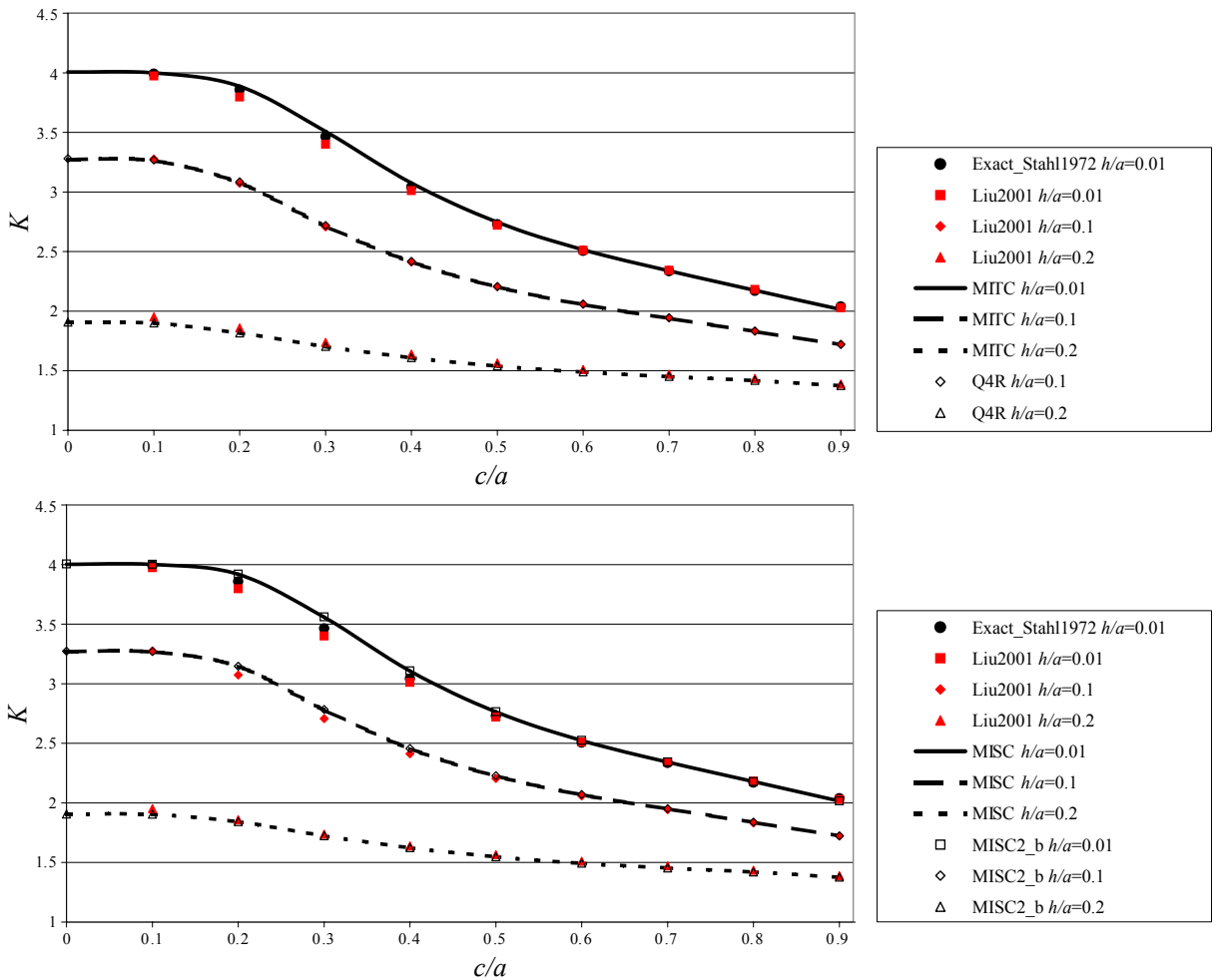


Figure 14. Buckling coefficients for rectangular ($a/b = 2$) edge cracked plates. Top: Q4R and MITC. Bottom: MISC2 and MISC2_b.

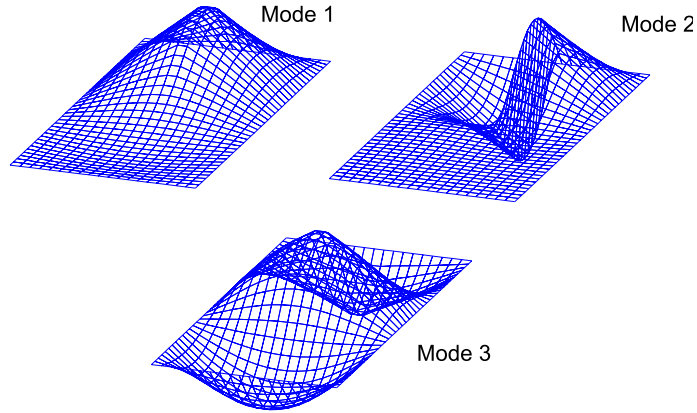


Figure 15. Buckling modes for simply supported edge cracked ($c/a = 0.5$) rectangular plate ($a/b = 2$).

Figure 14 also presents the analytical solution for thin cracked plates [Stahl and Keer 1972] and numerical solutions [Liu 2001]. In the majority of cases, very good agreement ($\sim 1\%$) was obtained with the reported results. The largest difference ($\sim 3\%$) with the reported data occurs for short-medium crack sizes ($a/c = 0.2, 0.3, 0.4, 0.5$), particularly for the MISC2 and MISC2_b elements. The first 3 buckling modes for a thin ($h/a = 0.01$) edge cracked ($c/a = 0.5$) rectangular plate ($a/b = 2$) are shown in Figure 15.

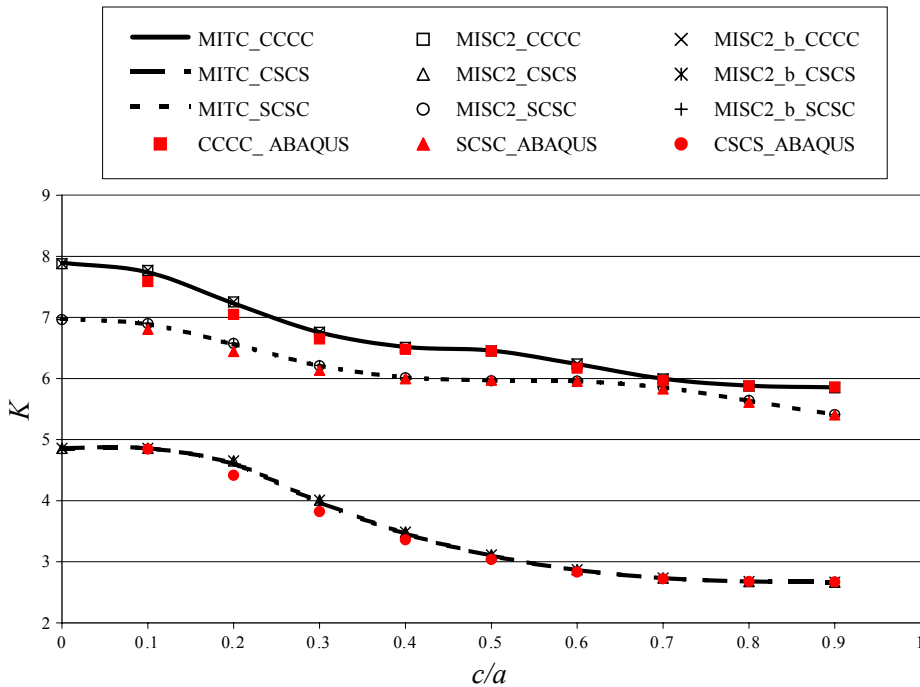


Figure 16. Buckling coefficients for rectangular ($a/b = 2$) centre cracked plates with different boundary conditions.

6.6. Rectangular plate with a longitudinal centre crack under different boundary conditions. This last example considers different boundary conditions in a rectangular centre cracked thin plate. The boundary conditions for each case are given as follows:

- CCCC : Sides and ends clamped,
- SCSC : Sides clamped and ends simply supported,
- CSCS : Sides simply supported and ends clamped.

The aspect ratio of the plate is $a/b = 2$ and the plate thickness is $h/a = 0.01$, therefore only buckling coefficients for elements MITC, MISC2, and MISC2_b versus crack lengths (c/a) are presented in Figure 16 (as shown in the previous examples, element Q4R will exhibit locking under this condition). As expected each case of boundary conditions converges to the noncracked thin plate solutions ($c/a = 0$).

Figure 16 shows that as the crack size increases, buckling coefficients decrease for all the different boundary conditions. All the present results were obtained with an uniform mesh of 19×38 elements. In order to establish a comparison with standard FEM, symmetric ABAQUS models [ABAQUS 2009]

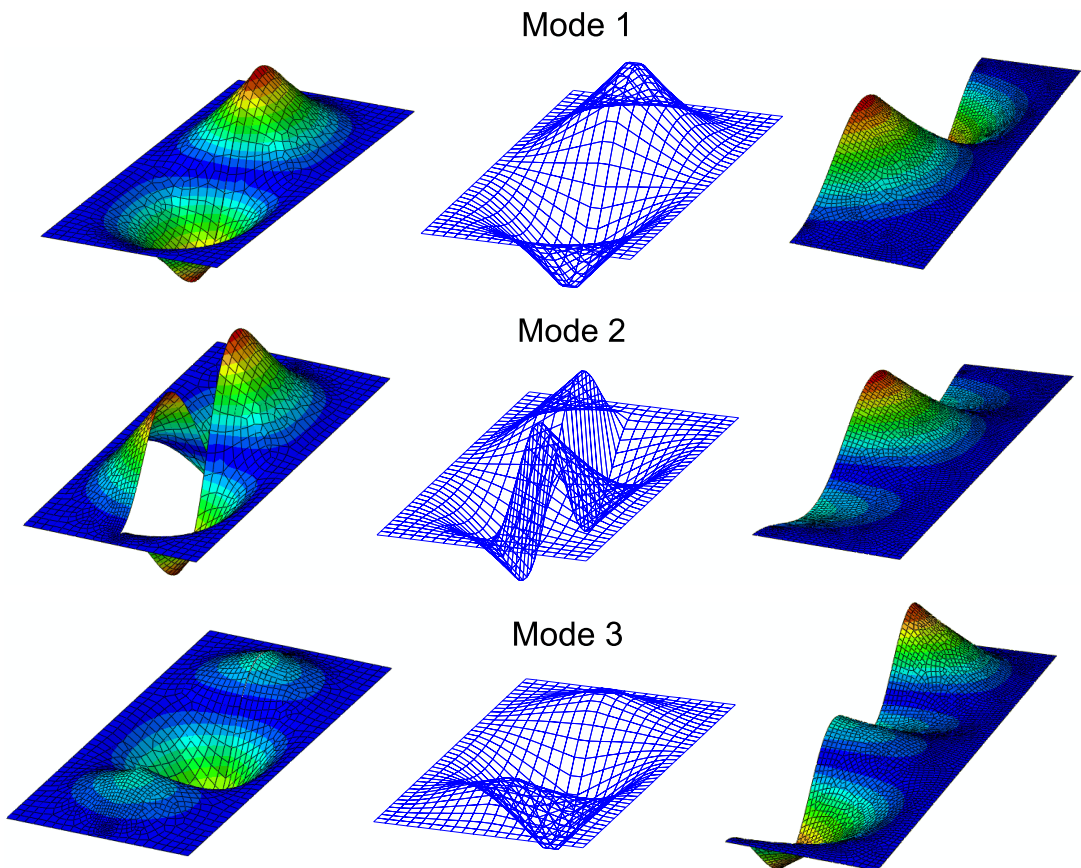


Figure 17. Buckling modes of clamped centre cracked ($c/a = 0.9$) rectangular plates ($a/b = 2$). Left: ABAQUS-seam model. Centre: XFEM model. Right: ABAQUS-symmetric model.

with an average of 4500 linear elements (S4R) are also plotted in [Figure 16](#). Totally clamped cracked plates exhibit the highest buckling coefficient. SCSC, as expected, gives higher buckling coefficients than CSCS, as the simply supported condition along the sides (see [Figure 3](#)) in the CSCS case provides a weaker constraint than in the SCSC case.

Buckling modes for the largest crack size ($c/a = 0.9$) and totally clamped boundary conditions are presented in [Figure 17](#). In this case, an additional ABAQUS model with a seam crack (ABAQUS-seam) is performed in order to compare buckling modes of full and symmetric models. It is clear from this figure the similarity in the first buckling mode for all cases. The second and third modes differ in the full and symmetric models as the antisymmetric opening mode (mode 2 in [Figure 17](#)) given by XFEM and ABAQUS-seam is not obtained in the symmetric ABAQUS model. Notice that the second mode in the ABAQUS symmetric solution corresponds to the third mode in the full models (XFEM and ABAQUS-seam).

7. Conclusions

In this paper, the smoothed extended finite element method was used to model the linear buckling response of uncracked and cracked isotropic shear deformable plates. Three different enriched elements were proposed: a stabilised MITC, a curvature smoothed MISC2, and a bending geometric stiffness matrix smoothed MISC2_b element. Each case corresponds to an extension of the previous. MISC2_b is an element only valid for linear plate buckling problems, and shows the influence of smoothing higher-order (nonlinear) terms. All enriched elements perform excellently (except for the Q4R element, which exhibits locking in the thin plate limit), with the MISC2 and MISC2_b elements providing slightly better results than the MITC element.

The effect of mesh distortion for uncracked and cracked plates was also considered, including the dependency on plate thickness. For distorted meshes, the classical Q4R element exhibits the worst performance, particularly for thin plates, while the newly proposed MISC2_b is shown to provide the most acceptable results for all cases (thin-thick and cracked-uncracked plates).

Two types of crack configurations have been considered in this study: a plate with a crack emanating from one edge, and a plate with a centrally located internal crack. Different plate thicknesses were considered, giving an overview of applications to thin and thick cracked plate buckling problems. It is seen that with increasing crack length and thickness, the buckling load decreases. Finally, different sets of boundary conditions were studied. It is worth noting that the present method greatly simplifies modelling of plate buckling with cracks, allowing us in some cases to provide antisymmetric crack opening modes that are not provided in classical symmetric FEM simulations, as shown with the totally clamped example.

References

- [ABAQUS 2009] *ABAQUS user's manual*, Version 6.9.1, Hibbitt, Karlsson and Sorensen, Pawtucket, Rhode Island, 2009.
- [Alinia et al. 2007] M. M. Alinia, S. A. A. Hosseinzadeh, and H. R. Habashi, "Numerical modelling for buckling analysis of cracked shear panels", *Thin-Walled Struct* **45**:12 (2007), 1058–1067.
- [Areias and Belytschko 2005] P. M. A. Areias and T. Belytschko, "Non-linear analysis of shells with arbitrary evolving cracks using XFEM", *Int. J. Numer. Meth. Eng.* **62**:3 (2005), 384–415.

- [Babuška et al. 1994] I. Babuška, G. Caloz, and J. E. Osborn, “Special finite element methods for a class of second order elliptic problems with rough coefficients”, *SIAM J. Numer. Anal.* **31**:4 (1994), 945–981.
- [Bachene et al. 2009] M. Bachene, R. Tiberkak, and S. Rechak, “Vibration analysis of cracked plates using the extended finite element method”, *Arch. Appl. Mech.* **79**:3 (2009), 249–262.
- [Bathe and Dvorkin 1985] K.-J. Bathe and E. N. Dvorkin, “A four-node plate bending element based on Mindlin/Reissner plate theory and a mixed interpolation”, *Int. J. Numer. Meth. Eng.* **21** (1985), 367–383.
- [Belytschko and Black 1999] T. Belytschko and T. Black, “Elastic crack growth in finite elements with minimal remeshing”, *Int. J. Numer. Meth. Eng.* **45**:5 (1999), 601–620.
- [Belytschko et al. 2009] T. Belytschko, R. Gracie, and G. Ventura, “A review of extended/generalized finite element methods for material modelling”, *Model. Simul. Mater. Sci. Eng.* **17**:4 (2009), 1–31.
- [Bordas and Natarajan 2010] S. P. A. Bordas and S. Natarajan, “On the approximation in the smoothed finite element method (SFEM)”, *Int. J. Numer. Meth. Eng.* **81**:5 (2010), 660–670.
- [Bordas et al. 2009] S. P. A. Bordas, T. Rabczuk, N. Hung, V. Nguyen, S. Natarajan, T. Bog, D. Quan, and N. Hiep, “Strain smoothing in FEM and XFEM”, *Comput. Struct.* **88**:23-24 (2009), 1419–1443.
- [Brighenti 2009] R. Brighenti, “Buckling sensitivity analysis of cracked thin plates under membrane tension or compression loading”, *Nucl. Eng. Des.* **239**:6 (2009), 965–980.
- [Dai et al. 2007] K. Y. Dai, G. R. Liu, and T. T. Nguyen, “An n -sided polygonal smoothed finite element method (n SFEM) for solid mechanics”, *Finite Elem. Anal. Des.* **43**:11-12 (2007), 847–860.
- [Dolbow et al. 2000] J. Dolbow, N. Moës, and T. Belytschko, “Modeling fracture in Mindlin–Reissner plates with the extended finite element method”, *Int. J. Solids Struct.* **37**:48-50 (2000), 7161–7183.
- [Gruttmann and Wagner 2004] F. Gruttmann and W. Wagner, “A stabilized one-point integrated quadrilateral Reissner–Mindlin plate element”, *Int. J. Numer. Methods Eng.* **61**:13 (2004), 2273–2295.
- [Hosseini-Hashemi et al. 2008] S. Hosseini-Hashemi, K. Khorshidi, and M. Amabili, “Exact solution for linear buckling of rectangular Mindlin plates”, *J. Sound Vibration* **315**:1-2 (2008), 318–342.
- [Le et al. 2010] C. V. Le, H. Nguyen-Xuan, H. Askes, S. P. A. Bordas, T. Rabczuk, and H. Nguyen-Vinh, “A cell-based smoothed finite element method for kinematic limit analysis”, *Int. J. Numer. Meth. Eng.* **83**:12 (2010), 1651–1674.
- [Liu 2001] F. L. Liu, “Differential quadrature element method for buckling analysis of rectangular Mindlin plates having discontinuities”, *Int. J. Solids Struct.* **38**:14 (2001), 2305–2321.
- [Liu 2010a] G. R. Liu, “A G space theory and a weakened weak (W^2) form for a unified formulation of compatible and incompatible methods, I: Theory”, *Int. J. Numer. Meth. Eng.* **81**:9 (2010), 1093–1126.
- [Liu 2010b] G. R. Liu, “A G space theory and a weakened weak (W^2) form for a unified formulation of compatible and incompatible methods, II: Applications to solid mechanics problems”, *Int. J. Numer. Meth. Eng.* **81**:9 (2010), 1127–1156.
- [Liu et al. 2007a] G. R. Liu, K. Y. Dai, and T. T. Nguyen., “A smoothed finite element method for mechanics problems”, *Comput. Mech.* **39**:6 (2007), 859–877.
- [Liu et al. 2007b] G. R. Liu, T. T. Nguyen, K. Y. Dai, and K. Y. Lam, “Theoretical aspects of the smoothed finite element method (SFEM)”, *Int. J. Numer. Meth. Eng.* **71**:8 (2007), 902–930.
- [Liu et al. 2009a] G. R. Liu, T. Nguyen-Thoi, and K. Y. Lam, “An edge-based smoothed finite element method (ES-FEM) for static, free and forced vibration analyses of solids”, *J. Sound Vibration* **320**:4-5 (2009), 1100–1130.
- [Liu et al. 2009b] G. R. Liu, T. Nguyen-Thoi, H. Nguyen-Xuan, and K. Y. Lam, “A node-based smoothed finite element method (N-SFEM) for upper bound solutions to solid mechanics problems”, *Comput. Struct.* **87**:1-2 (2009), 14–26.
- [Markström and Storåkers 1980] K. Markström and B. Storåkers, “Buckling of cracked members under tension”, *Int. J. Solids Struct.* **16**:3 (1980), 217–229.
- [Natarajan et al. 2009a] S. Natarajan, S. Bordas, and D. R. Mahapatra, “Numerical integration over arbitrary polygonal domains based on Schwarz–Christoffel conformal mapping”, *Int. J. Numer. Meth. Eng.* **80**:1 (2009), 103–134.
- [Natarajan et al. 2009b] S. Natarajan, S. P. A. Bordas, and T. Rabczuk, “Linear free flexural vibration of cracked isotropic plates using the extended finite element method”, preprint, 2009. Submitted to *Algorithms*.

- [Natarajan et al. 2010] S. Natarajan, D. R. Mahapatra, and S. P. A. Bordas, “Integrating strong and weak discontinuities without integration subcells and example applications in an XFEM/GFEM framework”, *Int. J. Numer. Meth. Eng.* **83**:3 (2010), 269–294.
- [Nguyen-Thanh et al. 2008] N. Nguyen-Thanh, T. Rabczuk, H. Nguyen-Xuan, and S. P. A. Bordas, “A smoothed finite element method for shell analysis”, *Comput. Methods Appl. Mech. Eng.* **198**:2 (2008), 165–177.
- [Nguyen-Xuan et al. 2008a] H. Nguyen-Xuan, S. Bordas, and H. Nguyen-Dang, “Smooth finite element methods: convergence, accuracy and properties”, *Int. J. Numer. Meth. Eng.* **74**:2 (2008), 175–208.
- [Nguyen-Xuan et al. 2008b] H. Nguyen-Xuan, T. Rabczuk, S. Bordas, and J. F. Debonoie, “A smoothed finite element method for plate analysis”, *Comput. Methods Appl. Mech. Eng.* **197**:13-16 (2008), 1184–1203.
- [Purbolaksono and Aliabadi 2005] J. Purbolaksono and M. H. Aliabadi, “Dual boundary element method for instability analysis of cracked plates”, *Comput. Model. Eng. Sci.* **8**:1 (2005), 73–90.
- [Rabczuk and Areias 2006] T. Rabczuk and P. Areias, “A meshfree thin shell for arbitrary evolving cracks based on an extrinsic basis”, *Comput. Model. Eng. Sci.* **16**:2 (2006), 115–130.
- [Rabczuk et al. 2007] T. Rabczuk, P. M. A. Areias, and T. Belytschko, “A meshfree thin shell method for non-linear dynamic fracture”, *Int. J. Numer. Meth. Eng.* **72**:5 (2007), 524–548.
- [Rabczuk et al. 2010] T. Rabczuk, R. Gracie, J.-H. Song, and T. Belytschko, “Immersed particle method for fluid-structure interaction”, *Int. J. Numer. Meth. Eng.* **81**:1 (2010), 48–71.
- [Reissner 1947] E. Reissner, “On bending of elastic plates”, *Quart. Appl. Math.* **5** (1947), 55–68.
- [Riks et al. 1992] E. Riks, C. C. Rankin, and F. A. Brogan, “The buckling behavior of a central crack in a plate under tension”, *Eng. Fract. Mech.* **43**:4 (1992), 529–548.
- [Sih and Lee 1986] G. C. Sih and Y. D. Lee, “Tensile and compressive buckling of plates weakened by cracks”, *Theor. Appl. Fract. Mech.* **6**:2 (1986), 129–138.
- [Stahl and Keer 1972] B. Stahl and L. M. Keer, “Vibration and stability of cracked rectangular plates”, *Int. J. Solids Struct.* **8** (1972), 69–91.
- [Vafai et al. 2002] A. Vafai, M. Javidruzi, and H. E. Estekanchi, “Parametric instability of edge cracked plates”, *Thin-Walled Struct.* **40**:1 (2002), 29–44.
- [Wang and Chen 2004] D. Wang and J.-S. Chen, “Locking-free stabilized conforming nodal integration for meshfree Mindlin–Reissner plate formulation”, *Comput. Methods Appl. Mech. Eng.* **193**:12-14 (2004), 1065–1083.
- [Wyart et al. 2007] E. Wyart, D. Coulon, M. Duflot, T. Pardoën, J.-F. Remacle, and F. Lani, “A substructured FE-shell/XFE-3D method for crack analysis in thin-walled structures”, *Int. J. Numer. Meth. Eng.* **72**:7 (2007), 757–779.

Received 28 Apr 2010. Revised 28 Sep 2010. Accepted 30 Nov 2010.

PEDRO M. BAIZ: p.m.baiz@imperial.ac.uk

Department of Aeronautics, Imperial College London, Prince Consort Road, London SW7 2AZ, United Kingdom

SUNDARARAJAN NATARAJAN: sundararajan.natarajan@gmail.com

School of Engineering, Cardiff University, Cardiff CF24 3AA, United Kingdom

STÉPHANE P. A. BORDAS: stephane.bordas@gmail.com

School of Engineering, Cardiff University, Cardiff CF24 3AA, United Kingdom

PIERRE KERFRIDEN: pierre.kerfriden@gmail.com

School of Engineering, Cardiff University, Cardiff CF24 3AA, United Kingdom

TIMON RABCZUK: timon.rabczuk@uni-weimar.de

Department of Civil Engineering, Bauhaus-Universität Weimar, 99421 Weimar, Germany

JOURNAL OF MECHANICS OF MATERIALS AND STRUCTURES

jomms.org

Founded by Charles R. Steele and Marie-Louise Steele

EDITORS

CHARLES R. STEELE Stanford University, USA
DAVIDE BIGONI University of Trento, Italy
IWONA JASIUK University of Illinois at Urbana-Champaign, USA
YASUHIRO SHINDO Tohoku University, Japan

EDITORIAL BOARD

H. D. BUI École Polytechnique, France
J. P. CARTER University of Sydney, Australia
R. M. CHRISTENSEN Stanford University, USA
G. M. L. GLADWELL University of Waterloo, Canada
D. H. HODGES Georgia Institute of Technology, USA
J. HUTCHINSON Harvard University, USA
C. HWU National Cheng Kung University, Taiwan
B. L. KARIHALOO University of Wales, UK
Y. Y. KIM Seoul National University, Republic of Korea
Z. MROZ Academy of Science, Poland
D. PAMPLONA Universidade Católica do Rio de Janeiro, Brazil
M. B. RUBIN Technion, Haifa, Israel
A. N. SHUPIKOV Ukrainian Academy of Sciences, Ukraine
T. TARNAI University Budapest, Hungary
F. Y. M. WAN University of California, Irvine, USA
P. WRIGGERS Universität Hannover, Germany
W. YANG Tsinghua University, China
F. ZIEGLER Technische Universität Wien, Austria

PRODUCTION contact@msp.org

SILVIO LEVY Scientific Editor

Cover design: Alex Scorpan

Cover photo: Mando Gomez, www.mandolux.com

See <http://jomms.org> for submission guidelines.

JoMMS (ISSN 1559-3959) is published in 10 issues a year. The subscription price for 2011 is US \$520/year for the electronic version, and \$690/year (+ \$60 shipping outside the US) for print and electronic. Subscriptions, requests for back issues, and changes of address should be sent to Mathematical Sciences Publishers, Department of Mathematics, University of California, Berkeley, CA 94720–3840.

JoMMS peer-review and production is managed by EditFLOW[®] from Mathematical Sciences Publishers.

PUBLISHED BY
 **mathematical sciences publishers**
<http://msp.org/>

A NON-PROFIT CORPORATION

Typeset in L^AT_EX

Copyright ©2011 by Mathematical Sciences Publishers

Journal of Mechanics of Materials and Structures

Volume 6, No. 9-10

November–December 2011

- Turtle shell and mammal skull resistance to fracture due to predator bites and ground impact** **DAVID L. HU, KELLY SIELERT and MICHAEL GORDON 1197**
- Linear buckling analysis of cracked plates by SFEM and XFEM** **P. M. BAIZ, S. NATARAJAN, S. P. A. BORDAS, P. KERFRIDEN and T. RABCUK 1213**
- A finite element for form-finding and static analysis of tensegrity structures**
DARIO GASPARINI, KATALIN K. KLINKA and VINICIUS F. ARCARO 1239
- Structural design of pyramidal truss core sandwich beams loaded in 3-point bending** **MING LI, LINZHI WU, LI MA, BING WANG and ZHENGXI GUAN 1255**
- Wave scattering from a rectangular crack in an anisotropic cladding**
PER-ÅKE JANSSON 1267
- Effect of adding crumb tire rubber particles on the mechanical properties of DCPD-modified sulfur polymer mortars**
HAMED MARAGHECHI, IMAN FOTOVAT AHMADI and SIAMAK MOTAHARI 1283
- Uniqueness theorems in the equilibrium theory of thermoelasticity with microtemperatures for microstretch solids**
ANTONIO SCALIA and MERAB SVANADZE 1295
- Implications of shakedown for design of actively cooled thermostructural panels**
NATASHA VERMAAK, LORENZO VALDEVIT, ANTHONY G. EVANS, FRANK W. ZOK and ROBERT M. MCMEEKING 1313